# Study of Allosteric Regulation of Escherichia coli Aspartate Transcarbamoylase

Author: Yunan Zheng

Boston College

The Graduate School of Arts and Sciences

Department of Chemistry

# Study of Allosteric Regulation of *Escherichia coli* Aspartate Transcarbamoylase

A THESIS

BY

YUNAN ZHENG

Submitted in partial fulfillment of the requirements

for the degree of Master of Science

October 2013

**Abstract**

For nearly 60 years the ATP activation and the CTP inhibition of *Escherichia coli* aspartate transcarbamoylase (ATCase) has been the textbook example of allosteric regulation. We present kinetic data and 5 X-ray structures determined in the absence and presence of a $Mg^{2+}$ concentration within the physiological range. In the presence of 2 mM divalent cations ($Mg^{2+}$, $Ca^{2+}$, $Zn^{2+}$) CTP does not significantly inhibit the enzyme while the allosteric activation by ATP is enhanced. The data suggest that the actual allosteric inhibitor *in vivo* of ATCase is the combination of CTP, UTP and a $M^{2+}$ cation and the actual allosteric activator is ATP and $M^{2+}$ or ATP, GTP and $M^{2+}$. The structural data reveals that two NTPs can bind to each allosteric site with a $Mg^{2+}$ ion acting as a bridge between the triphosphates. Thus the regulation of ATCase is far more complex than previously believed and calls many previous studies into question. The X-ray structures reveal the catalytic chains undergo essentially no alternations, however, several regions of the regulatory chains undergo significant structural changes. Most significant is that the N-terminal regions of the regulatory chains exist in different conformations in the allosterically activated and inhibited forms of the enzyme. Here, a new model of allosteric regulation is proposed.

**Acknowledgement**

I would first like to give my deepest gratitude to my research advisor, Dr. Kantrowitz, for his guidance, research direction, and insight. His passion for science is contagious and I am thankful to him for inspiring me to work in this fascinating research area that was totally new to me. I truly appreciate that Dr. Kantrowitz gave me the chance to work in his lab. I am grateful to him for all the advice and tremendous help he gave regarding my research and this thesis. I would also like to thank my fellow research group members, past and present: Kate, I must thank you for everything you have taught me and the encouragement you have given me, which are important for me to carry on my research career. Greg, thank you for helping me with the crystallography software and other programs, and for being an excellent research mentor. Judy, thank you for your willingness to help whenever I needed anything. I also thank my parents and Brian Sneed for everything they have done to help. It would not be possible for me to make it this far without the love and support of my family and friends. Finally, I would like to express my gratitude to the committee members: Dr. Kantrowitz, Dr. Chatterjee, Dr. Gao. Thank you for your valuable time and comments on my thesis.

**Abbreviations**

| | |
|---|---|
| ATCase | aspartate transcarbamoylase |
| CP | carbamoyl phosphate |
| Asp | L-aspartate |
| PALA | N-phosphonoacetyl-L-aspartate |
| PDB | Protein Data Bank |
| MWC | Monad, Wyman and Chaangeux |
| RMSD | root-mean-square deviation |
| 50s loop | residues 46-58 of the regulatory chain |
| 130s loop | resides 129-134 of the regulatory chain |
| T state | low activity, low affinity tense state |
| R state | high activity, high affinity relax state |
| c1 and c6 | catalytic chains in the asymmetric unit |
| r1 and r6 | regulatory chains in the asymmetric unit |
| SAXS | small-angle X-ray scattering |
| NTP | nucleotide triphosphate |

**Table of Contents**

# Introduction

## Nucleotides and Divalent Metal

Nucleotides play a variety of important roles in all cells and are essential to life. A nucleotide is composed of a phosphate, a ribose sugar and either a purine or pyrimidine base (Figure 1). ATP and GTP are purine triphosphate nucleotides while CTP, UTP, TTP are pyrimidine triphosphate nucleotides. It is well known that these nucleotides are the components of genetic information, present as the activated precursors of DNA and RNA. They are also involved in a great number of intracellular and intercellular functions. For example, GTP, guanosine triphosphate, serves as substrate in the signal transduction pathways. Signal transduction by G-protein coupled receptors (GPCRs), transmembrane proteins, involves a conformational change upon binding of GTP to the proteins.[1] The hydrolysis of ATP, adenosine triphosphate, provides a lot of energy thus it is the universal currency of energy in biological systems, and it is the most abundant among the nucleotides.[2] Similar to ATP, CTP and UTP are also high-energy molecules. One of the roles of CTP and UTP is feedback inhibition of one of the enzyme required to catalyze the committed step in the pyrimidine biosynthesis pathway, the reaction catalyzed by aspartate transcarbamoylase, therefore maintaining a balance in the pyrimidine pool.[3]

Divalent metals, such as $Mg^{2+}$, exist at high concentration in cells, are important for plants and animals and also are involved in numerous enzymatic reactions. For example, chlorophyll, responsible for the green color of plants, has a $Mg^{2+}$ coordinated to the clorin. $Mg^{2+}$ is also required in the process of DNA replication, serving as essential cofactor in the DNA polymerase reaction.[4]

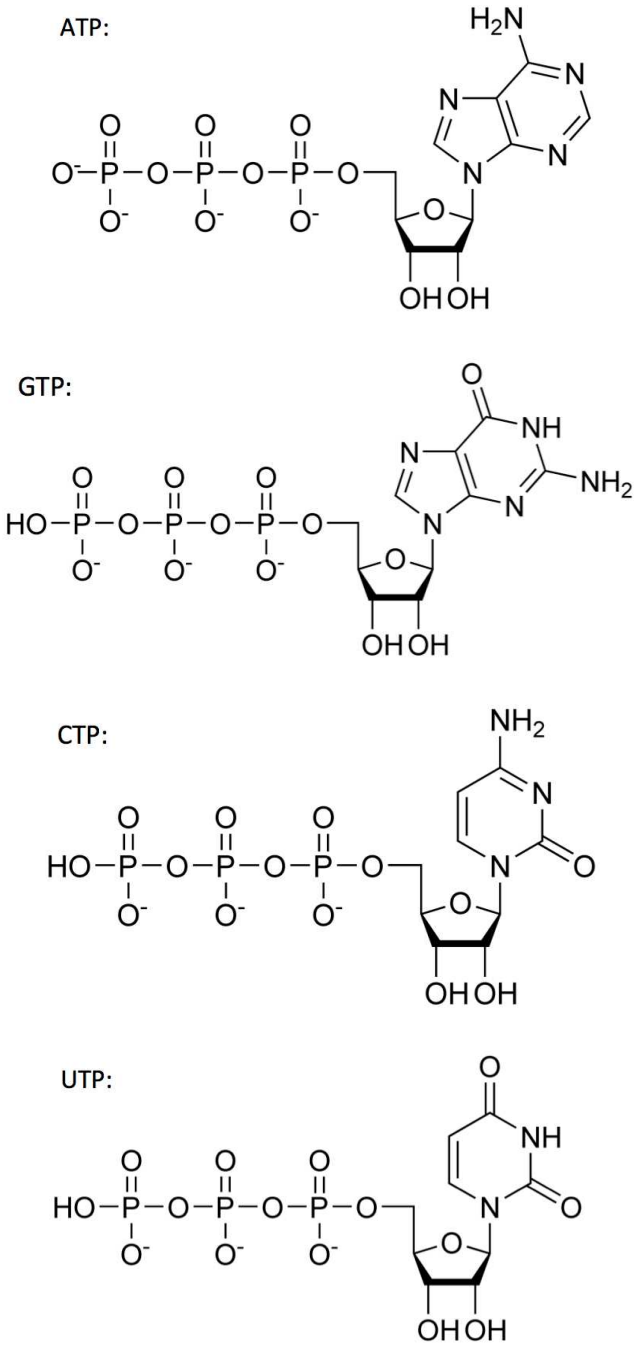


**Figure 1.** Chemical Structures of ATP, GTP, CTP and UTP center structures

In case of aspartate transcarbamoylase, both nucleotides and divalent metals together regulate its activity. Numerous studies have been performed to illustrate how the functionality of the enzyme is regulated, including structural crystallography analysis, small angle X-ray scattering, site-directed mutagenesis and kinetic studies. Although the important role of the nucleotides effectors is well accepted, the mode by which different nucleotides bring about different modes of regulation is still unclear. In this study a variety of methods are used to better understand the role of metal ions in the regulation of aspartate transcarbamoylase.

## Aspartate Transcarbamoylase

### Homotropic Cooperativity

Aspartate transcarbamoylase (ATCase) catalyzes the first reaction of the pyrimidine biosynthetic pathway, which is the carbamylation of the amino group of aspartate by carbamoyl phosphate (Figure 2).[5] The *E. coli* ATCase holoenzyme (310 kDa) is composed of two catalytic trimers (34 kDa) and three regulatory dimers (17 kDa), arranged along a 3-fold axis of symmetry (Figure 3). Both the catalytic and regulatory chains have two structural domains.[6] Each catalytic chain consists of the aspartate (Asp) domain and carbamoyl phosphate (CP) domain, which bind to the substrates aspartate and carbamoyl phosphate, respectively. Each regulatory chain consists of two domains, the allosteric (Al) domain and zinc (Zn) domain, which contains the allosteric binding site and structural Zn atom, respectively. ATCase exists in an equilibrium[7] between two states that are defined by changes in the tertiary and quaternary structures: a low activity, low affinity for substrates taut (T-state) structure, and a high activity, high affinity for substrates relaxed (R-state) form. The main rigid body movements of the subunits describing the quaternary structure transition include an 11 Å vertical expansion along the 3-fold axis, and a 12 degree rotation of the catalytic trimers relative to each other around this axis, along with a 15 degree rotation of each of the three regulatory dimers around the 2-fold axes.[8] In the absence of substrates, the [T]/[R] ratio is about 250 thus the equilibrium favors the T state.[9] Binding of the substrates, or substrate analogs (e.g. N-phosphonoacetyl-L-aspartate; PALA) (Figure 2) shifts the equilibrium from T to R in a concerted fashion. The transition between the T state and R state of ATCase can be explained by the Monod, Wyman, Changeux (MWC) model.[10] In this model, the binding

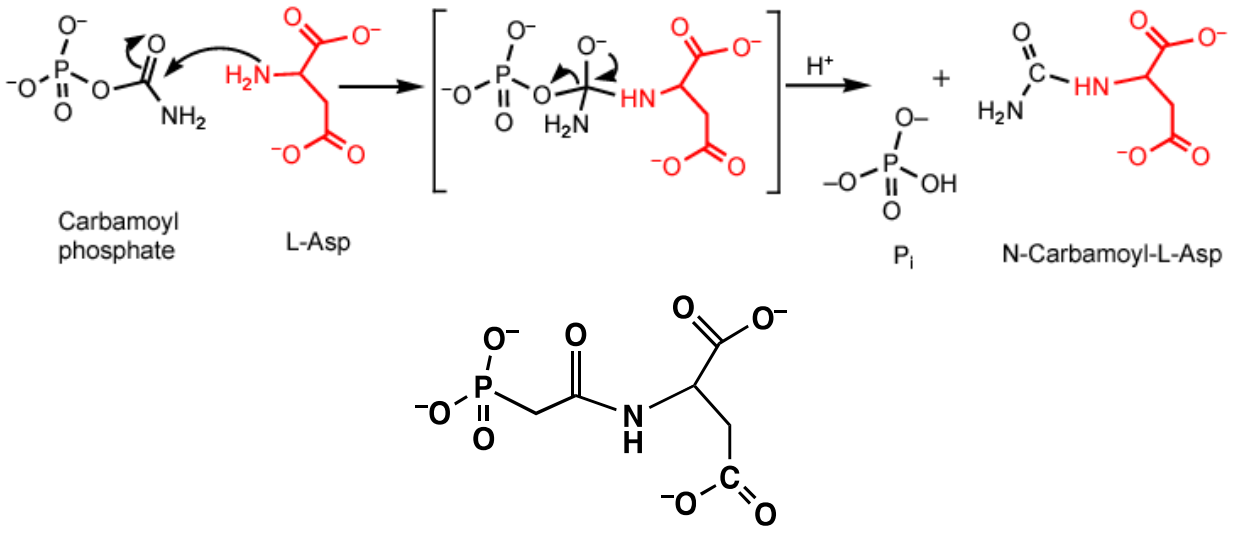


N-phosphonoacetyl-L-aspartate; PALA

**Figure 2.** Carbamoylation Reaction catalyzed by ATCase

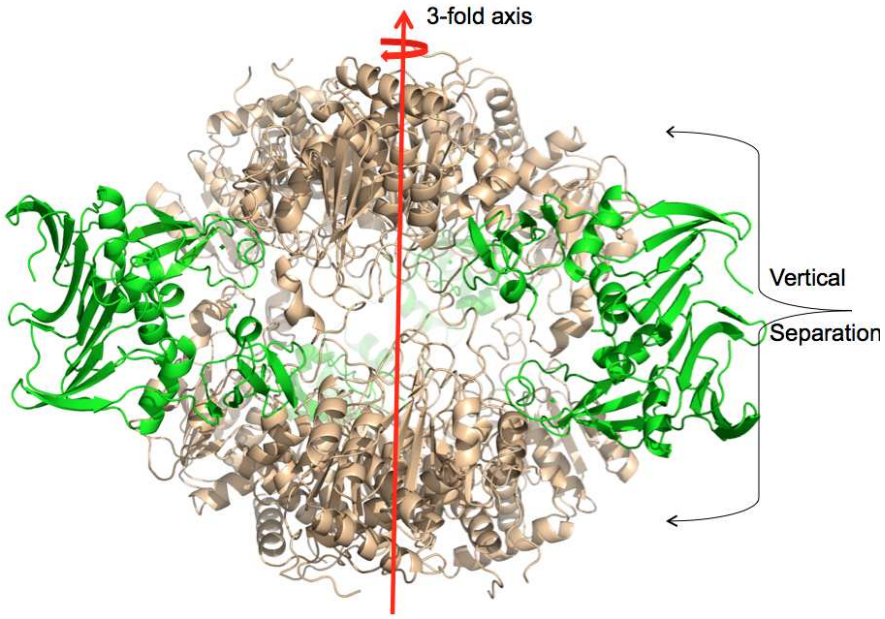


**Figure 3A.** Structure of *E. coli* ATCase holoenzyme. The bronze colored subunits represent the catalytic chains. The green colored subunits represent the regulatory chains. This figure is drawn by PyMol using PDB ID 1D09. By measuring the distance between the center mass of the catalytic trimers, vertical separation shows a ~11 Å elongation along the 3-fold axis when the enzyme goes from T state to R state.

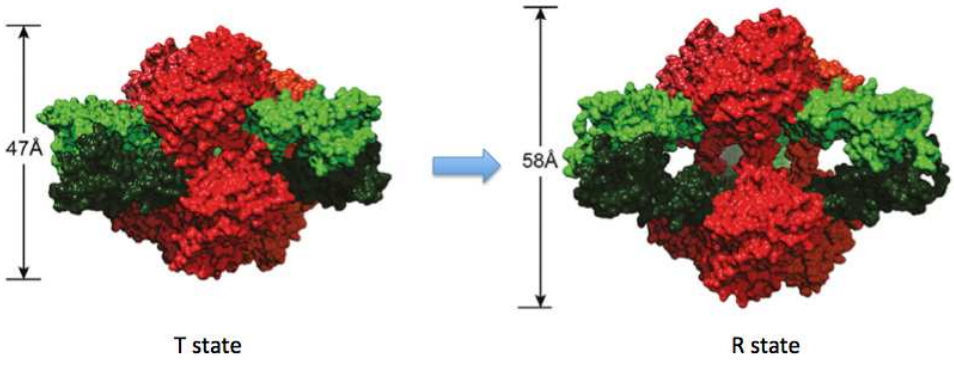


**Figure 3B**. Quaternary conformational changes from T state to R state. Both structures are drawn by PyMol using PDB ID 1D09 for the R state and PDB ID 1ZA1 for the T state.

of one ligand to the enzyme induces conformational changes that are propagate to all the other subunits. Therefore all subunits of the enzyme exit in the same conformation and the transition is concerted. The MWC model explains the transition of ATCase from T state to R state during catalysis. The reaction catalyzed by ATCase follows an ordered-binding mechanism.[11] First, the substrate CP binds to the active site, which induces local conformational changes around the active site allowing the second substrate Asp to bind while the enzyme still remains in T state. Next, Asp binds to the active site, induces the quaternary conformational changes converting the entire enzyme to R state. Thus, the Asp saturation curve for ATCase exhibits homotropic cooperativity.[12] In addition, small-angle X-ray scattering has shown that the binding of PALA to one of the six active sites was sufficient to induce a concerted transition of the entire molecule to the R state[13] providing supports that ATCase follows the MWC model.

**Heterotropic Regulation**

ATCase is also heterotropically regulated by allosteric effectors[14], and has been used as a model for allosteric regulation. Allosteric regulation occurs when a small natural compound binds to the enzyme at a site other than the substrate-binding site. These compounds are known as allosteric effectors, and they regulate the activity of enzyme. In *E. coli* ATCase, the allosteric site in the regulatory chain is located approximately 60Å from the active site in the catalytic chain. Aside from the homotropic regulation by its substrate aspartate; pyrimidine and purine nucleotides heterotropically regulate ATCase where ATP enhances the activity of ATCase while CTP and UTP synergistically inhibit it. Binding of CTP to the allosteric site greatly increases the [T]/[R] to 1250, thus shifting

the equilibrium towards the T state, while the binding of ATP to the same allosteric site significantly decreases the [T]/[R] to 70, thus shifting the equilibrium toward the R state.[9] This shift in equilibrium explains the decreased activity of the enzyme in the presence of CTP and the increased activity of the enzyme in the presence of ATP at a fixed concentration of aspartate. The regulatory nucleotides cannot induce the transition from the T to the R state, although they do alter the equilibrium between the two states.

Each of the allosteric effectors has been shown to have an enhanced kinetic response when bound with a synergistic effector. In the case of CTP, the synergistic effector UTP decreases the activity of ATCase in the presence of CTP more than CTP alone.[3] The synergistic inhibition of ATCase by the combination of CTP and UTP reduces the enzyme activity by approximately 95%. In the case of ATP, the synergistic effector $Mg^{2+}$ increases the activity of ATCase in the presence of ATP substantially more than ATP alone.[15] In fact, ATP•$Mg^{2+}$ has been postulated to cause a more elongated R state of ATCase by small-angle X-ray scattering in solution.[15]

**One Regulatory Chain Has Two Nucleotide Binding Site**

Mendes et al.[16] studied the allosteric effects of nucleotide binding to ATCase through the incorporation of an unnatural fluorescent amino acid close to the allosteric site of the enzyme. The functional mutant enzyme was generated via incorporation of the fluorescent amino acid, L-(7-hydroxycoumarin-4-yl)ethylglycine (HCE-Gly) into position 52 on the regulatory chain using procedures developed in the Schultz laboratory[17]. Analysis of fluorescence binding isotherms indicated that CTP and UTP

bind independently, suggesting that CTP and UTP do not compete for the same binding site.

Recent, structural studies of ATCase with UTP bound have revealed more information about how nucleotides bind to the allosteric sites.[18] The X-ray structural analysis of the *E. coli* ATCase bound with UTP showed that each regulatory chain contains one allosteric site composed of the A and B subsites. Previous studies showed CTP and ATP compete for a same site,[19] and this site has been defined as the A subsite. The B site, located directly adjacent to the A site, is where UTP binds. Two UTP can bind together filling both subsites in the presence of $Mg^{2+}$.

Another study by our group on the synergistic inhibition of ATCase by UTP in the presence of CTP uncovered that the presence of a metal ion (e.g. $Mg^{2+}$) was critical for synergistic inhibition.[3] In this study, dCTP was used as a surrogate for CTP to determine the structure of the enzyme in the presence of both dCTP and UTP. This structure revealed that the allosteric site of each regulatory chain could bind two nucleotides simultaneously with a divalent cation coordinated between the β and  phosphates of each nucleotide (see Figure 4). CTP or dCTP bind in essentially the same manner to the A subsite and UTP binds to the B subsite. This work also showed that in the absence of divalent cations UTP was unable to synergistically inhibit ATCase in the presence of CTP. Based upon these data, a new model of allostery for *E. coli* ATCase was proposed. In this model, the B site acts as an amplification site and the nucleotide in the B site will only amplify the kinetic response from the nucleotide bound in the A site if a metal ion is present. This amplified response was theorized to be an effect of a stronger shift in equilibrium between the T and R states when two nucleotides and a metal ion occupied

the allosteric site than if only one nucleotide was bound. It was speculated that this new model could explain the enhanced activity of the enzyme in the presence of ATP•$Mg^{2+}$ as compared to ATP alone. Our studies show that in the presence of $Mg^{2+}$, two ATP molecules bind together in the allosteric site of ATCase, one in each subsite, with a $Mg^{2+}$ coordinated between their phosphate groups.

This thesis presents the results and analysis of 5 structures of ATCase, obtained by X-ray crystallography, in the R state with nucleotides bound in the presence or absence of $Mg^{2+}$: ATCase•CTP•$Mg^{2+}$•UTP, ATCase•ATP•$Mg^{2+}$•ATP, ATCase•UTP•$Mg^{2+}$•UTP, ATCase•ATP, ATCase•CTP. In addition, we use kinetics studies to investigate the role of divalent cations on the allosteric regulation. We chose $Mg^{2+}$, $Cu^{2+}$ and $Zn^{2+}$ because of their highly abundant existence in the cells.

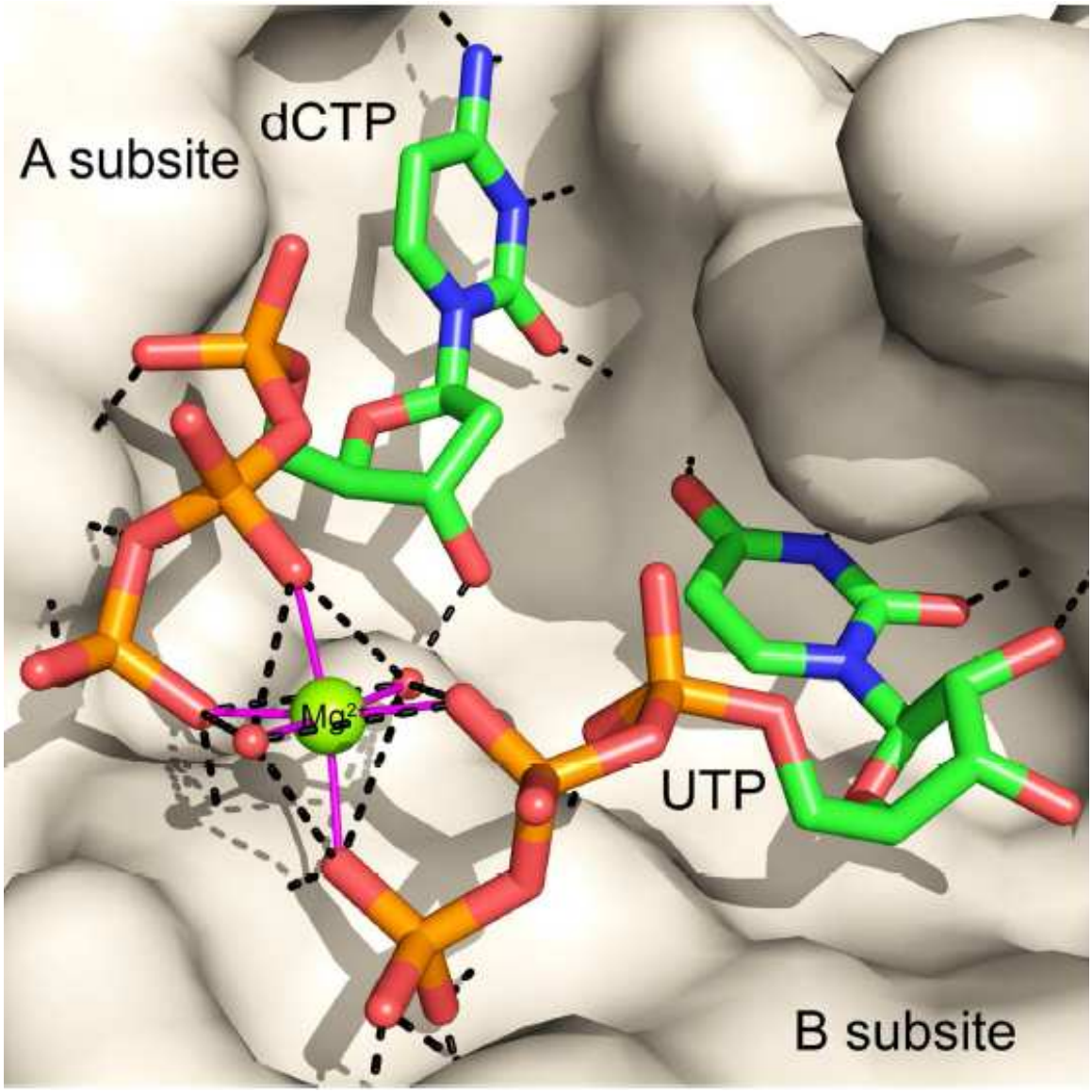


**Figure 4.** T-state X-ray crystal structure of ATCase in the presence of dCTP, UTP and $Mg^{2+}$. The r6 regulatory subsites A and B are shown as a surface representation. dCTP is in the A subsite and UTP is in the B subsite. The $Mg^{2+}$ is shown as a green sphere and coordinated ligand interactions are shown with magenta lines. Hydrogen-bonding interactions to the enzyme and waters are shown as dash lines (black). Water ligands to $Mg^{2+}$ are shown as red spheres. This figure was drawn with CHIMERA[20] using PDB ID 4FYX[3].

## Reference


1. Bhattacharya, M., Babwah, A.V., Ferguson, S. S. (2004) *Biochem. Soc. Trans*.*32*, Small GTP-binding protein-coupled receptors, 1040-1044
2. Buckstein, M. H., He, J., Rubin, H. (2008), Characterization of nucleotide pools as a function of physiological state in Escherichia coli. *J. Bacteriol, 190(2),* 718-728
3. Cockrell, G. M., Kantrowitz, E. R. (2012) Metal Ion Involvement in the Allosteric Mechanism of *Escherichia coli* Aspartate Transcarbamoylase, *Biochemistry 51,* 7128-7137
4. Yang, L., Arora, K., Beard, W. A., Wilson, S. H., Schlick, T., (2004) Critical role of magnesium ions in DNA polymerase beta's closing and active site assembly, J. Am. Chem. Soc. 126(27), 8441-53
5. Reichard, P., Hanshoff, G. (1956) Aspartate carbamyl transferase from *Escherichia coli*, *Acta Chem. Scand. 10*, 548-560.
6. Krause, K. L., Voltz, K. W., Lipscomb, W. N. (1987) 2.5 Å structure of aspartate carbamoyltransferase complexed with the bisubstrate analog N-(phosphonacetyl)-L-aspartate, *J. Mol. Biol. 193*, 527-553.
7. Fetler, L., Kantrowitz, E. R., Vachette, P. (2007) Direct observation in solution of pre-existing structure equilibrium for a mutant of allosteric aspartate transcarbamoylase, *Proc. Natl. Acad. Sci. U. S. A. 104*, 495-500.
8. Jin, L., Stec, B., Lipscomb, W. N., Kantrowitz, E. R. (1999) Insights into the mechanism of catalysis and heterotropic regulation of *E. coli* aspartate transcarbamoylase based upon a structure of enzyme complexed with the

bisubstrate analog N-phosphonacetyl-L-aspartate at 2.1 Å, *Proteins: Struct. Funct. Genet. 37*, 729-742.

9. Howlett, G. J., Blackburn, M. N., Compton, J. G., Schachman, H. K. (1977) Allosteric regulation of aspartate transcarbamoylase. Analysis of the structural and functional behavior in terms of a two-state model, *Biochemistry 16*, 5091-5099.

10. Monod, J., Wyman, J., Changeux, J. P. (1965) On the Nature of Allosteric Transitions: A Plausible Model, *J. Mol. Biol. 12*, 88-118.

11. Wang, J., Stieglitz, K. A., Cardia, J. P., Kantrowitz, E. R. (2005) Structural basis for ordered substrate binding and cooperativity in aspartate transcarbamoylase, *Proc. Natl. Acad. Sci. U. S. A. 102*, 8881-8886.

12. Newton, C. J., Kantrowitz, E. R. (1990) The regulatory subunit of *Escherichia coli* aspartate carbamoyltransferase may influence homotropic cooperativity and heterotropic interactions by a direct interaction with the loop containing residues 230-245 of the catalytic chain, *Proc. Natl. Acad. Sci. U. S. A. 87*, 2309-2313.

13. Macol, C. P., Tsuruta, H., Stec, B., Kantrowitz, E. R. (2001) Direct structural evidence for a concerted allosteric transition in *Escherichia coli* aspartate transcarbamoylase, *Nat. Struc. Biol. 8*, 423-426.

14. Christopherson, R. I., and Finch, L. R. (1977) Regulation of aspartate carbamoyltransferase of *Escherichia coli* by the interrelationship of magnesium and nucleotides, *Biochim. Biophys. Acta 481*, 80-85.

15. Fetler, L., and Vachette, P. (2001) The allosteric activator Mg-ATP modifies the quaternary structure of the R-state of *Escherichia coli* aspartate transcarbamylase without altering the TR equilibrium, *J. Mol. Biol. 309*, 817-832.

16. Mendes, K. R., Martinez, J. A., and Kantrowitz, E. R. (2010) Asymmetric allosteric signaling in aspartate transcarbamoylase, *ACS Chem. Biol. 5*, 499-506.

17. Wang, J., Xie, J., Schultz, P. (2006) A genetically encoded fluorescent amino acid, *J. Am. Chem. Soc. 128*, 8738–8739.

18. Peterson, A. W., Cockrell, G. M., and Kantrowitz, E. R. (2012) A second allosteric site in *E. coli* aspartate transcarbamoylase, *Biochemistry 51*, 4776-4778.

19. Gouaux, J. E., Stevens, R. C., Lipscomb, W. N. (1990) Crystal structures of aspartate carbamoylase ligated with phosphoacetamide, malonate, and CTP or ATP at 2.8 Å and neutral pH, *Biochemistry 29*, 7702-7715.

20. Pettersen, E. F., Goddard, T. D., Huang, C. C., Couch, G. S., Greenblatt, D. M., Meng, E. C., and Ferrin, T. E. (2004) UCSF Chimera - A visualization system for exploratory research and analysis, *J. Comput. Chem. 25*, 1605-1612.

# A New Paradigm for Allosteric Regulation of Escherichia coli Aspartate Transcarbamoylase

## Material And Methods

### Materials

Ampicillin, magnesium chloride hexahydrate, UTP, glycine, glucose, EDTA, agar, L-aspartate, N-carbamoyl-L-aspartate, 2-mercaptoethanol, and uracil were obtained from Sigma-Aldrich (St. Louis, MO). CTP and 2-bis(2-hydroxyethyl)amino-2-(hydroxymethyl)-1,3-propanediol (Bis-Tris) were from Santa Cruz Biotechnology, Inc. (Santa Cruz, CA). Tris, N-cyclohexyl-3-aminopropanesulfonic acid (CAPS), electrophoresis-grade acrylamide, enzyme-grade ammonium sulfate and GTP were from MP Biomedicals (Santa Ana, CA). Antipyrine, diacetylmonoxime, sodium molybdate dihydrate, tryptone and yeast extract were obtained from Fisher (Pittsburgh, PA). Casamino acid was from Becton, Dickinson and Company (Franklin Lakes, NJ). Agarose, ammonium persulfate, sodium dodecyl sulfate, coomassie brilliant blue and Chelex 100 resin were purchased from Bio-Rad (Hercules, CA). The carbamoyl phosphate dilithium salt obtained from Sigma-Aldrich was purified before use by precipitation from 50% (v/v) ethanol and was stored desiccated at -20° C.[1]

## Enzyme Expression and Purification

*E. coli* ATCase was overexpressed in M9 media supplemented with 5 g/L casamino acids using *E. coli* strain EK1104[2] [$F^-$ *ara*, *thi*, Δ(*pro-lac*), Δ*pyrB*, *pyrF*$^{\pm}$, *rpsL*] transformed with plasmid pEK152[3] containing the *E. coli pyrBI* gene. The isolation and

purification was as previously described.[4] Enzyme concentrations were determined by absorbance measurements at 280 nm with an extinction coefficient of 0.59 $cm^2/mg$.[5]

## Determination of ATCase Activity

Activity measurement with the nucleotide effectors ATP, CTP, GTP and UTP were performed in the absence and presence of $Mg^{2+}$, $Ca^{2+}$, and $Zn^{2+}$ at 28° C. Pretreatment of nucleotides with Chelex 100 resin (Bio-Rad) were carried out to remove cation contamination in the commercial supply. Chelex 100 resin was added to each nucleotide solution (0.05 g per 1 mL). The mixture was stirred gently on ice for 1 hr. Resin was removed by centrifugation and the nucleotide solution with metal removed was obtained as supernatant. When required, $MgCl_2$, $CaCl_2$, or $ZnCl_2$ were added to adjust the $M^{2+}$ concentration.

The concentration of the nucleotide triphosphates was determined spectrophotometrically at pH 7.0 using previously reported values of molar absorptivity.[6] The activity of the transcarbamoylase reaction was determined colorimetrically[7] in a tri-part buffer containing 20 mM Bis-Tris, 20 mM Tris, and 20 mM CAPS or a Tris buffer containing 50 mM Tris, at pH 7.0 or pH 8.3, respectively, in the presence of a saturating concentration of carbamoyl phosphate (2.0 mM). Specific activity is in units of mM N-carbamoyl-L-aspartate•$min^{-1}$•$mg^{-1}$. The L-aspartate concentration was varied from 0 to 80 mM and 0 to 100 mM at pH 7.0 and pH 8.3, respectively for the data in Figure 6[8] and the concentration of wild-type ATCase varied from $3 \times 10^{-5}$ to $30 \times 10^{-5}$ mg/ml. The values reported are the average of four determinations. Fitting of the experimental data to theoretical equations was accomplished by nonlinear regression. Data is shown in Table 1.

**Table 1.** Influence of Allosteric Effectors on the Relative Activity[a] of ATCase in the Absence and Presence of $Mg^{2+}$.

| | | $Mg^{2+}$ (mM)[d] | | |
|---|---|---|---|---|
| NTP[b] | Reported Value[c] | 0 | 1.0 | 2.0 |
| none | 1.0 | 1.0 | 1.0 | 1.0 |
| ATP | 1.35 | 1.29 ± 0.07 | 1.33 ± 0.07 | 1.52 ± 0.13 |
| CTP | 0.43 | 0.49 ± 0.01 | 0.80 ± 0.05 | 0.97 ± 0.05 |
| UTP | 0.95 | 0.99 ± 0.01 | 0.97 ± 0.01 | 0.89 ± 0.04 |
| GTP | 0.71 | 0.95 ± 0.05 | 0.61 ± 0.06 | 0.84 ± 0.04 |
| ATP + CTP | 0.85 | 0.87 ± 0.02 | | 1.25 ± 0.03 |
| ATP + UTP | 1.52 | 1.40 ± 0.06 | | 1.43 ± 0.06 |
| ATP + GTP | 1.58 | 1.38 ± 0.04 | | 1.57 ± 0.05 |
| CTP + UTP | 0.06 | 0.47 ± 0.10 | | 0.12 ± 0.04 |
| CTP + GTP | 0.58 | 0.61 ± 0.08 | | 0.81 ± 0.15 |
| UTP + GTP | 0.84 | 0.68 ± 0.01 | | 0.75 ± 0.02 |

[a] Relative activity was determined by dividing the value of specific activity of ATCase in the presence of nucleotide(s) by that in the absence of nucleotide(s).

[b] All nucleotide concentrations were 2 mM.

[c] The relative activities reported by Wild *et al*. [9]

[d] All experiments were performed at 28 °C in 20 mM Bis-Tris, 20 mM Tris, and 20 mM CAPS buffer, pH 7.0 at saturating carbamoyl phosphate (2 mM) and 5 mM aspartate. The values reported are the average of four determinations.

## Crystallization, X-ray Data Collection, and Processing

*E. coli* ATCase (10 mg/mL) was placed in 50 μL dialysis buttons (Hampton Research, Aliso Viejo, CA) and dialyzed against 20 mL of crystallization buffer (50 mM maleic acid, 1 mM PALA, and 3 mM sodium azide, pH 5.90) at 20° C.[10] Crystals formed in about 1 week with average dimensions of 0.6 x 0.2 x 0.2 mm. Dialysis buttons were transferred to 1 mL of crystallization buffer with either 5 mM CTP, 5 mM ATP, 5 mM each of ATP and $MgCl_2$, 5 mM each of UTP and $MgCl_2$, or 5 mM each of CTP, UTP and $MgCl_2$, and allowed to equilibrate for 12 hours. The crystals were dipped in crystallization buffer with 5 mM each of the matching nucleotide and $MgCl_2$ with 20% (v/v) 2-methyl-2,4-pentandiol as a cryo-protectant for approximately 1 minute prior to flash freezing.

The data for the crystals soaked in CTP alone, UTP•$Mg^{2+}$, and ATP•$Mg^{2+}$ were collected on beamline X29 at the National Synchrotron Light Source at Brookhaven National Laboratory (Upton, NY), while the data for crystals soaked in the presence ATP alone and CTP•$Mg^{2+}$•UTP were collected with a Rigaku MicroMax-07 HF high-intensity microfocus rotating Cu anode X-ray generator coupled with Osmic VariMax Optics and a R-Axis $IV^{++}$ image plate area detector that is part of the Boston College Crystallography Facility. The diffraction data were integrated, scaled, and averaged using either HKL2000[11] or d*TREK (Rigaku/MSC).[12] Data collection and refinement statistics are shown in Table 2.

## Table 2. Data Collection and Refinement Statistics[a]

| | $R_{PALA}$•ATP | $R_{PALA}$•CTP | $R_{PALA}$•UTP•$Mg^{2+}$•UTP | $R_{PALA}$•ATP•$Mg^{2+}$•ATP | $R_{PALA}$•CTP•$Mg^{2+}$•UTP |
|---|---|---|---|---|---|
| ***Data collection statistics*** | | | | | |
| PDB entry | 4KGV | 4KGX | 4KGZ | 4KH0 | 4KH1 |
| Space Group | P321 | P321 | P321 | P321 | P321 |
| Wavelength | 1.542 | 1.075 | 1.075 | 1.075 | 1.542 |
| Cell Dimensions | | | | | |
| *a* = *b, c* (Å) | 121.1, 155.5 | 121.2, 154.7 | 121.4, 155.1 | 121.1, 155.1 | 120.9, 154.7 |
| *α*, *β*, *γ* (°) | 90, 90, 120 | 90, 90, 120 | 90, 90, 120 | 90, 90, 120 | 90, 90, 120 |
| Resolution (Å) | 38.4 - 2.1 (2.2 - 2.1) | 50 - 2.2 (2.3 - 2.2) | 50 - 2.4 (2.5 - 2.4) | 50 - 2.25 (2.33 - 2.25) | 31.8 - 2.2 (2.3 - 2.2) |
| $R_{sym}$[b] | 0.05 (0.38) | 0.08 (0.65) | 0.11 (0.68) | 0.09 (0.74) | 0.04 (0.37) |
| Average (I/σ) | 12.8 (3.3) | 19.9 (3.9) | 14.6 (3.7) | 21.8 (3.7) | 17.8 (3.8) |
| Completeness (%) | 100.0 (100.0) | 100.0 (99.9) | 100.0 (100.0) | 100.0 (100.0) | 99.4 (100.0) |
| Redundancy | 5.3 (5.3) | 22.4 (18.9) | 24.1 (21.2) | 24.1 (22.0) | 5.7 (5.6) |

***Refinement statistics***

| | | | | | |
|---|---|---|---|---|---|
| Resolution (Å) | 38.4 - 2.1 | 49.7 - 2.2 | 49.8 - 2.4 | 49.7 - 2.25 | 31.8 - 2.2 |
| Reflections | 77,282 | 67,081 | 52,387 | 62,983 | 66,367 |
| $R_{work}/R_{free}$ | 0.168 / 0.208 | 0.156 / 0.192 | 0.165 / 0.203 | 0.168 / 0.208 | 0.163 / 0.196 |
| Number of atoms | | | | | |
| Protein | 7,098 | 7,082 | 7,074 | 7,202 | 7,132 |
| Waters | 688 | 683 | 339 | 467 | 458 |
| RMS deviations | | | | | |
| Bond lengths (Å) | 0.007 | 0.007 | 0.009 | 0.007 | 0.008 |
| Angles (°) | 1.07 | 1.07 | 1.09 | 1.13 | 1.08 |
| Mean B value ($Å^2$) | 48.3 | 39.3 | 56.9 | 48.2 | 60.2 |

[a] Values in parentheses are for the highest resolution shell.

[b] $R_{sym} = \sum|(I - \langle I \rangle)|/\sum(I)$, where I is the observed intensity.

## Structure Solution and Data Refinement

Each structure was solved using phases from the $R_{PALA}$ structure (PDB ID: 1D09)[13] as the initial model after removal of water and ligand molecules. Automated refinements using translation libration screw-motion (TLS) parameters were performed in PHENIX after an initial rigid body refinement.[14] Manual rebuilding, addition of waters, and nucleotide modeling were performed using COOT.[15] Waters were accepted if they were within hydrogen-bonding distance of main-chain or side-chain atoms. The final structures were validated using MolProbity[14] and PROCHECK.[16] Coordinates and structure factors for the $R_{PALA}$•ATP, $R_{PALA}$•CTP, $R_{PALA}$•UTP•$Mg^{2+}$•UTP, $R_{PALA}$•ATP•$Mg^{2+}$•ATP, and $R_{PALA}$•CTP•$Mg^{2+}$•UTP complexes have been deposited in the Protein Data Bank under accession codes 4KGV, 4KGX, 4KGZ, 4KH0, 4KH1, respectively.

## Calculation of Small-Angle X-ray Scattering Profiles

X-ray scattering patterns were calculated from the experimental X-ray crystal data using the fast SAXS profile computation with Debye formula (FOXS) server (http://modbase.compbio.ucsf.edu/foxs). The FoXS server explicitly computes all inter-atomic distances as well as models the first solvation layer based upon the atomic solvent accessible areas.[17] Hydrogen atoms were considered implicitly. For consistency, the first 9 residues of each regulatory chain were not included in the calculations.

## Results and Discussion

### Influence of $Mg^{2+}$ on the Allosteric Response of ATCase

Although it has been known for almost 50 years that divalent cations influence the allosteric regulation of ATCase[18-20], the mechanism by which divalent cations alter the allosteric response has remained elusive. In fact, under a physiological concentration of ATP, 3.6 mM,[21] $Mg^{2+}$•ATP activates ATCase 2.9-fold as compared to 1.9-fold for ATP alone.[20] Kung et al.[22] have estimated that the intercellular concentrations of $Mg^{2+}$ and $Ca^{2+}$ are greater than 20 mM, and $Zn^{2+}$ about 5-fold lower. Since the dissociation constant of $M^{2+}$•NTP complexes is in the micromolar range, most of the NTPs in the cell will be present as $M^{2+}$•NTP complexes. Therefore, it is more reasonable to consider how ATCase responds to the NTPs in the presence rather than the absence of $M^{2+}$.

To ensure that the NTPs did not contain trace amounts of metal ions, all NTP solutions were pretreated. In order to directly compare our data to that of Wild et al.[9] we used identical buffer, pH and Asp concentrations. Figure 5 and Table 3 shows the influence of $Mg^{2+}$ on the activity of the enzyme in the presence of various NTPs and NTP combinations. Complete substrate saturation curves are shown in Figure 6.

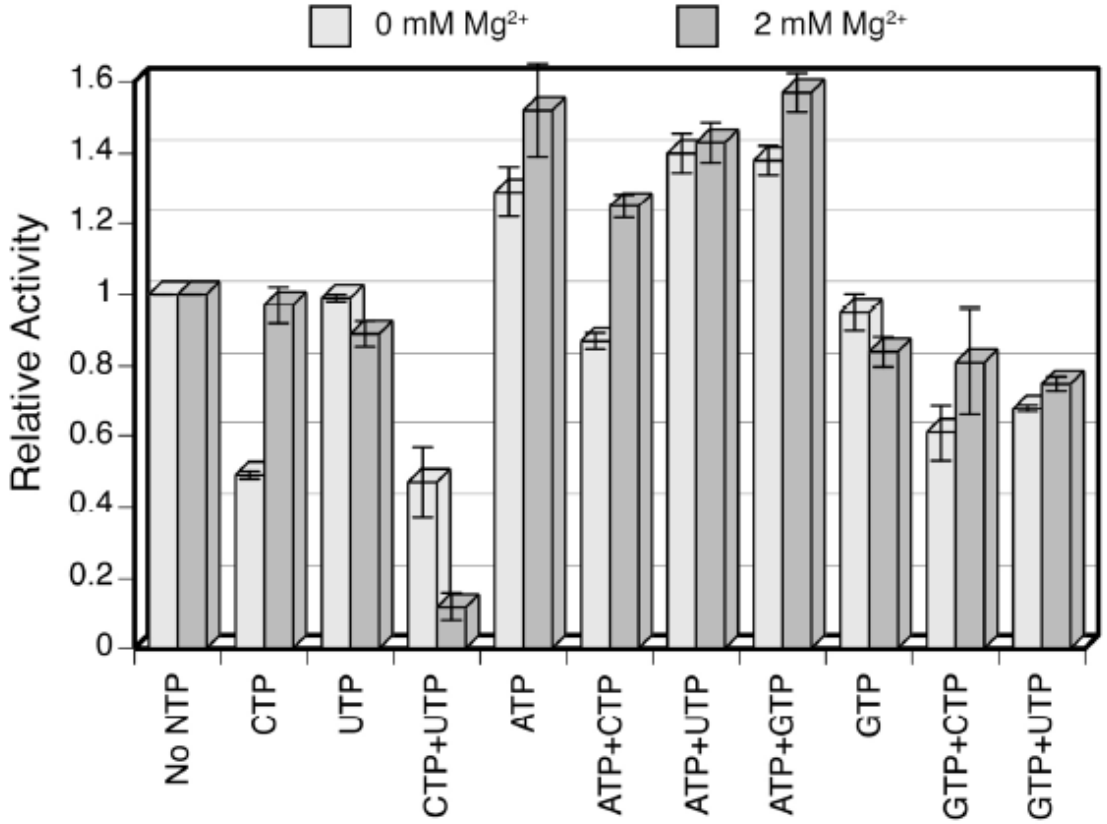


**Figure 5**. Influence of allosteric effectors on the activity of ATCase in the absence and presence of $Mg^{2+}$ at pH 7. Relative activity was determined in the absence or presence of 2 mM $Mg^{2+}$. Measurements with single nucleotides were performed at 2 mM, while measurements with pairs were performed at 1 mM each. Assay conditions used were identical to those used by Wild et al.[9] except that the NTPs were treated to remove trace metals before use. Data used for this figure are provided in Table 3.

**Table 3.** Influence of Allosteric Effectors on the Relative Activity of ATCase in the Absence and Presence of Divalent Cations.[a]

| | Relative Activity | | |
|---|---|---|---|
| NTP | $Mg^{2+}$ (2 mM) | $Ca^{2+}$ (2 mM) | $Zn^{2+}$ (2 mM) |
| none | 1.0 | 1.0 | 1.0 |
| ATP | 1.52 ± 0.13 | 1.48 ± 0.04 | 1.31 ± 0.06 |
| CTP | 0.97 ± 0.05 | 0.83 ± 0.03 | 0.75 ± 0.02 |
| CTP + UTP | 0.19 ± 0.07 | 0.12 ± 0.08 | 0.23 ± 0.08 |

[a] All experiments were performed at 28° C in 20 mM Bis-Tris, 20 mM Tris, and 20 mM CAPS buffer, pH 7.0 at saturating carbamoyl phosphate (2 mM) and 5 mM aspartate. The values reported are the average of four determinations.

[b] Relative activity was determined by dividing the value of specific activity of ATCase in the presence of nucleotide(s) by that in the absence of nucleotide(s).

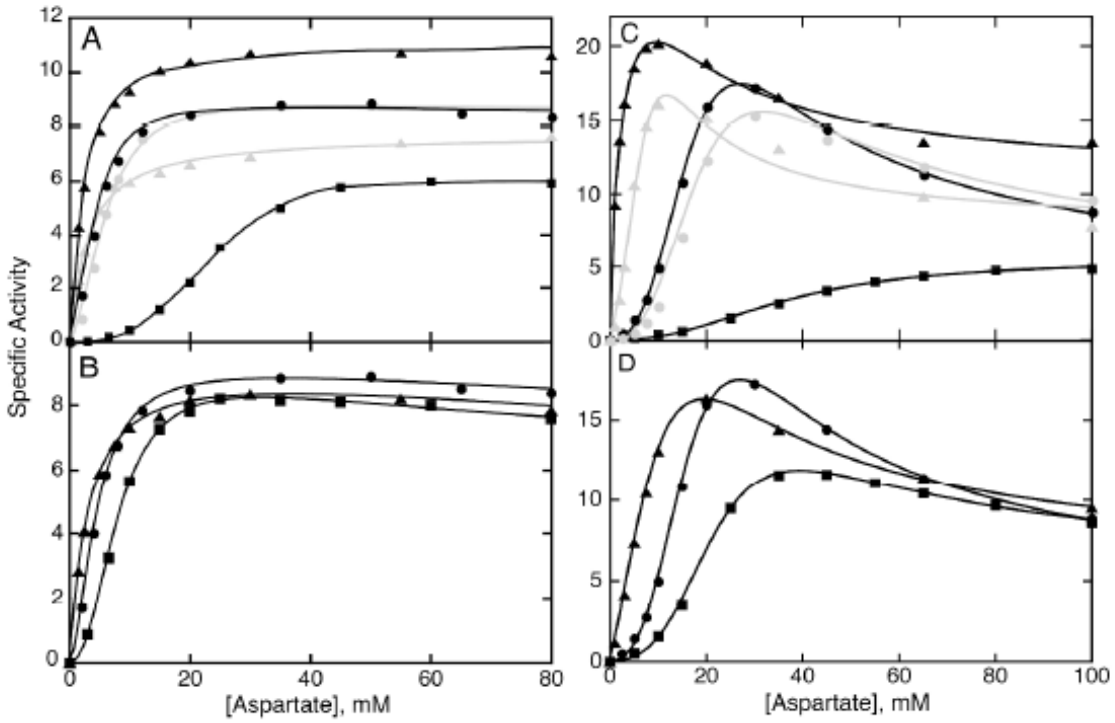


**Figure 6.** Asp saturation curves in the presence of NTPs and $Mg^{2+}$ at pH 7.0 (A, B) and pH 8.3 (C, D). (A, C) Data are shown in the absence of NTPs and in the absence (circle, black) or presence of 2 mM $Mg^{2+}$ (circle, gray), in the presence of 2 mM CTP, 2 mM UTP and 2 mM $Mg^{2+}$ (square, black), in the presence of 2 mM ATP, 2 mM GTP and 2 mM $Mg^{2+}$ (triangle, black) and in the presence of 4 mM ATP and 2 mM $Mg^{2+}$ (triangle, gray). (B, D) Asp saturation curves in the absence (circle) and presence of ATP (triangle) and CTP (square) in the absence of $Mg^{2+}$. Specific activity, mM carbamoyl aspartate•$min^{-1}$•$mg^{-1}$, at 28º C was determined colorimetrically at a saturating concentration of carbamoyl phosphate (2 mM) and 2 mM $MgCl_2$ in 20 mM Bis-Tris, 20 mM Tris, and 20 mM CAPS buffer at pH 7.0 and 50 mM Tris at pH 8.3.

CTP can inhibit ATCase in the absence of $Mg^{2+}$, however, CTP has little influence on activity in the presence of 2 mM $Mg^{2+}$ suggesting a reduced role of CTP in the allosteric regulation of ATCase *in vivo*. However, in the presence of $Mg^{2+}$, the combination of the two end products of the pyrimidine pathway, CTP and UTP, inhibit the enzyme almost completely. It is known that CTP competitively inhibits its own production by binding to CTP synthetase, which would elevate the levels of UTP.[9] The combination of CTP, UTP and $Mg^{2+}$ as the natural allosteric inhibitor of ATCase would thus help to maintain an overall balance in relative pyrimidine and purine nucleotide pools without disrupting the balance between the CTP and UTP pools.

ATP is able to activate the enzyme in the absence of $Mg^{2+}$, however in the presence of $Mg^{2+}$, ATP activates the enzyme to a greater extent (Figure 5). Furthermore, using small-angle X-ray scattering in solution, Fetler et al.[20] have reported that the R-state enzyme undergoes a significantly larger structural change with ATP in the presence of $Mg^{2+}$ than in its absence. ATP and GTP activates the enzyme slightly more than ATP alone (see Figure 5). However, at higher concentrations of Asp, the addition of GTP to ATP and $Mg^{2+}$substantially increases the activity (see Figure 6). Buckstein et al.[21] have determined concentrations of ATP, GTP, UTP and CTP in mid-log phase *E. coli* to be 3.56, 1.66, 0.67 and 0.33 mM respectively. These intracellular concentrations suggest that both end products of purine nucleotide biosynthesis, ATP and GTP, are involved in the allosteric regulation of ATCase.

These results are most relevant due to the high intercellular $Mg^{2+}$ concentration, however other divalent cations such as $Ca^{2+}$ and $Zn^{2+}$ were also found to cause very similar nucleotide responses as $Mg^{2+}$ (see Table 3).

**Structures of ATCase with NTPs in the Presence and Absence of $Mg^{2+}$**

Five structures of ATCase were determined in the presence of N-phosphonacetyl-L-aspartate (PALA) to induce the R state. The ATP ($R_{PALA}$•ATP) and CTP ($R_{PALA}$•CTP) were determined in the absence of divalent cations as controls. The remaining three structures are NTP and $Mg^{2+}$ combinations including: ATP•$Mg^{2+}$, CTP•UTP•$Mg^{2+}$ and UTP•$Mg^{2+}$ of which activate, inhibit the enzyme to the greatest extent and has little influence on activity, respectively. A summary of the data collection and refinement statistics are provided in Table 1.

The addition of any NTP and independent of the presence of $Mg^{2+}$ induces almost no structural alterations to the catalytic chains. As shown in Table S3, the average RMSD between the catalytic chains of the $R_{PALA}$ structure and the catalytic chains of each of the NTP structures determined was only 0.69 ± 0.05 Å. In contrast the average RMSD between the regulatory chains of the $R_{PALA}$ structure and the regulatory chains of each of the NTP structures determined was 1.41 ± 0.16 Å. Thus, the binding of the nucleotides has a significantly larger structural influence on the regulatory than the catalytic chains. The addition of any NTP with or without $Mg^{2+}$ induces larger alterations in the r6 chains (RMSD 1.04 ± 0.28 Å) than the r1 chains (0.77 ± 0.07 Å) reinforcing the previously observed asymmetry in the regulatory dimer.[23]

During the T to R allosteric transition the enzyme expands by approximately 11 Å along the three-fold axis, as well as rotates around the 2 and 3-fold axes. The vertical separation[24] of ATCase is a measure of the distance between the centers of mass of the upper and lower catalytic trimers. The vertical separation of the T state structure (PDB code 1ZA1) is 47.3 Å compared to 57.9 Å for the R-state structure ($R_{PALA}$, PDB code

1D09). The corresponding vertical separations for the $R_{PALA}$•ATP, $R_{PALA}$•CTP, $R_{PALA}$•UTP•$Mg^{2+}$•UTP, $R_{PALA}$•ATP•$Mg^{2+}$•ATP, $R_{PALA}$•CTP•$Mg^{2+}$•UTP are 57.5, 57.2, 57.4, 57.4 and 57.3 Å respectively. Thus, the quaternary structure of all the structures determined here have the characteristic vertical separation of the R state of ATCase. None of the NTPs in the absence or presence of $Mg^{2+}$ cause an appreciable alteration in the quaternary structure of the enzyme.

The binding of the various NTP•$Mg^{2+}$ combinations did not induce any significant alterations to the positions of side chains in the active site, although this may be due to the high affinity of PALA orienting the active site residues. Since the NTP•$Mg^{2+}$ combinations do not significantly alter the activity of the enzyme at saturating concentrations of the substrates (see Figure 6), either the presence of PALA in the active site makes any conformational changes or the NTPs alter the enzyme activity by binding to the allosteric site and preferentially stabilize the T or R states.

All the structures reported in the presence of $Mg^{2+}$, $R_{PALA}$•ATP•$Mg^{2+}$•ATP, $R_{PALA}$•CTP•$Mg^{2+}$•UTP and $R_{PALA}$•UTP•$Mg^{2+}$•UTP show electron density in the allosteric site corresponding to nucleotides bound in both the A and B subsites with a $Mg^{2+}$ in between. As an example, shown in Figure 7 is the r6 allosteric site of the $R_{PALA}$•ATP•$Mg^{2+}$•ATP structure, additional details can be seen in Figure S1. The $Mg^{2+}$ is octahedrally coordinated to six oxygen atoms; two from water molecules, and one from the β-phosphate and the γ-phosphate of each of the two NTPs in the A and B subsites. The water molecules coordinated to the $Mg^{2+}$ have additional stabilizing interactions with β and γ phosphate oxygens (see Figure 7B). Thus, the allosteric site of ATCase has two subsites capable of binding NTPs.

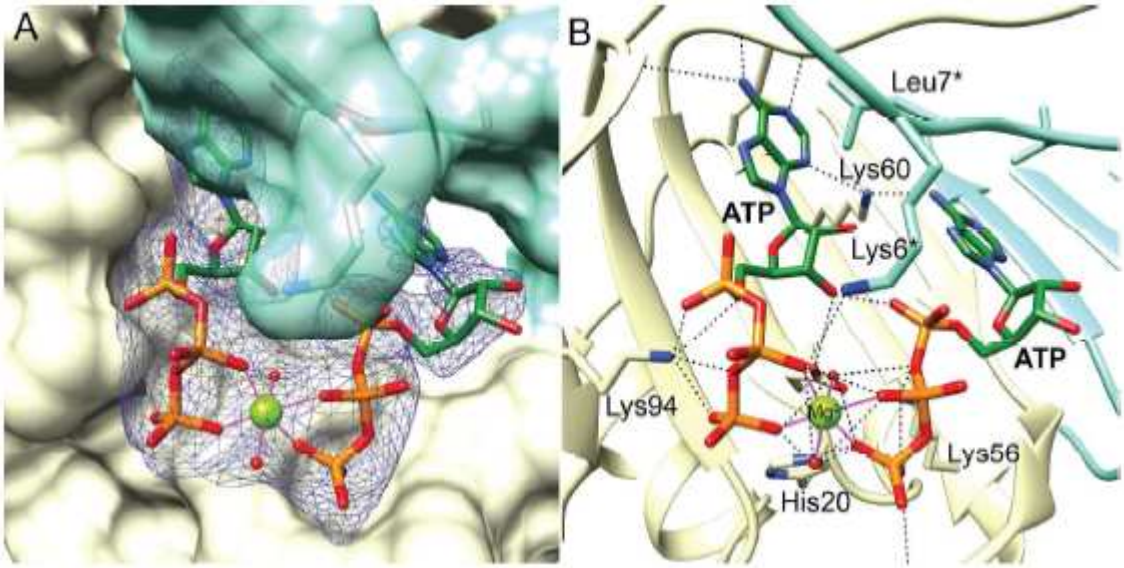


**Figure 7**. Allosteric site of ATCase with ATP and $Mg^{2+}$. (A) Surface representation of the r6 regulatory site with the r1 chain in blue (with transparency) and the r6 chain in yellow. Shown in dark blue is the electron density map at 2.5 σ calculated by omitting the atoms of the two ATPs, $Mg^{2+}$ and waters. (B) Same view as in (A) showing the interactions between the two ATPs and $Mg^{2+}$ with the enzyme. Residues with asterisks are from the r1 chain.

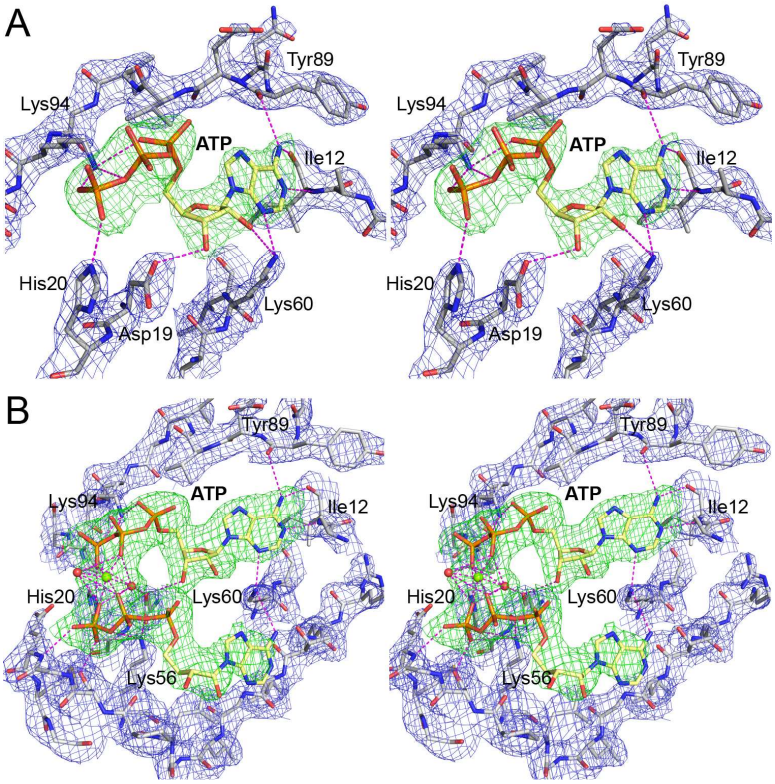


**Fig. S1**. The allosteric site with ATP and ATP•$Mg^{2+}$ bound with electron density. Stereoviews of r6 regulatory site of ATCase with ATP bound in (A) the absence, and (B) the presence of $Mg^{2+}$. Shown is the electron density (blue) at 1.0 σ with the final coordinates of the atoms overlaid. Shown in green is the electron density map at 4.0 σ calculated by omitting the atoms of the ATP, or ATP and $Mg^{2+}$, from the calculations. Hydrogen bonding interactions are shown as dash lines (magenta).

As seen in Figure 8A and 8B, only one subsite is filled in the absence of a divalent cation. ATP and CTP bind competitively to the A subsite while UTP binds only to the B subsite as previously reported.[25] Previous studies have shown that the concentration of CTP necessary to half inhibit the enzyme is approximately 6-fold lower than the concentration of ATP needed to activate the enzyme.[26] The higher affinity of the enzyme for CTP compensates for the approximately 10-fold higher concentration of ATP in cells[21] allowing the two nucleotides to compete more equally.

Examination of the $R_{PALA}$•ATP•$Mg^{2+}$•ATP reveals that the interactions between the enzyme and ATP in the A subsite are very similar to those between the enzyme and ATP in the $R_{PALA}$•ATP structure determined in the absence of $Mg^{2+}$ (compare Figures 8A and 8D). The phosphates of ATP bound in the B subsite interact with the backbone nitrogen of Glu52 as well as the side chains His20, Ser50 and Lys56, all of which are involved in the binding of UTP in the B subsite (compare Figures 8D and 8F). The ε-amino of Lys60 exhibits a water-mediated interaction and a polar interaction with the N7 and 6-amino group of the adenine ring, respectively (Figure 8D). However, in the B subsite of the adjacent regulatory chain there is a direct interaction between Lys60 and N7.

The allosteric site of the $R_{PALA}$•CTP•$Mg^{2+}$•UTP structure is shown in Figure 8E. CTP was modeled into the A subsite and UTP was modeled into the B subsite based upon the subsite specificity previously determined.[4] The 4-amino group of the cytosine in the A subsite acts as a hydrogen bond donor to the backbone carbonyls of Ile12 and Tyr89. Furthermore, all the interactions to CTP observed in the $R_{PALA}$•CTP structure in the absence of $Mg^{2+}$ are also observed in the $R_{PALA}$•CTP•$Mg^{2+}$•UTP structure (compare Figures 8B and 8E).

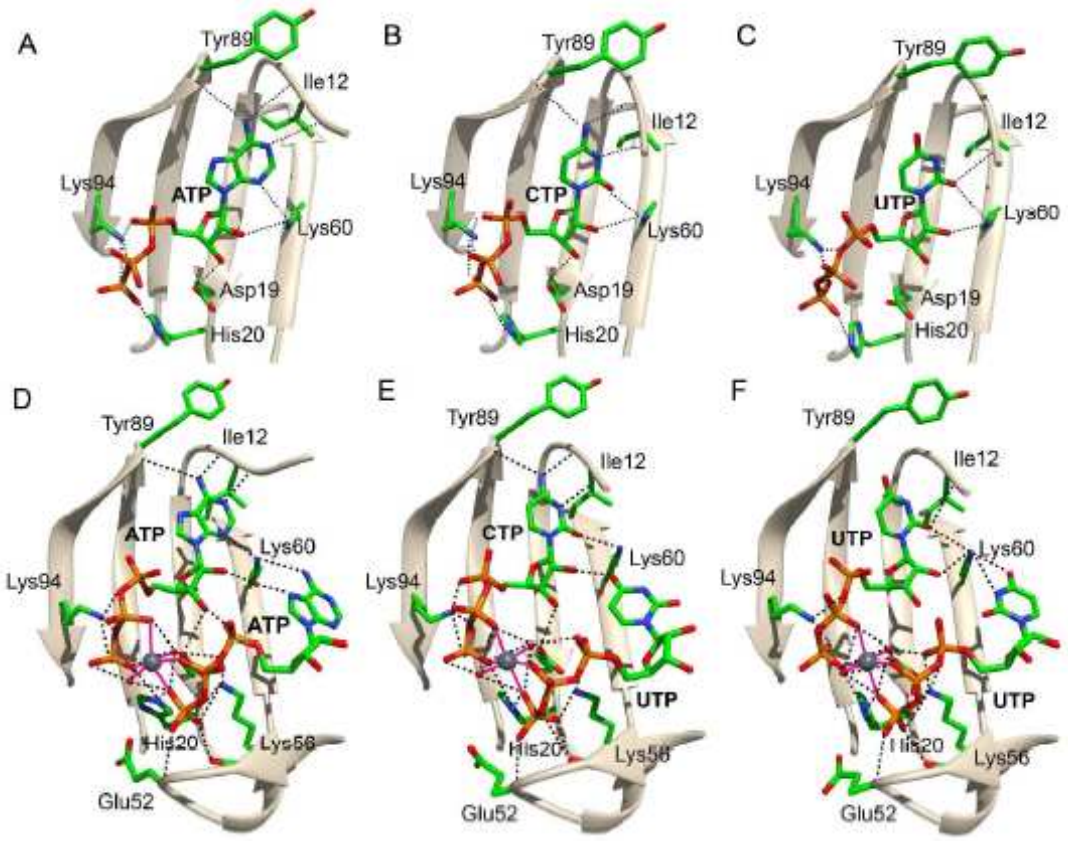


**Figure 8.** (Top) Structural comparison of ATP, CTP and UTP bound in the A subsite. ATP (A), CTP (B) and UTP (C) are shown in A subsite of the r6 regulatory domain of ATCase. In the case of UTP (C), the A subsite is only occupied in the presence of $Mg^{2+}$ (not shown). Hydrogen-bonding interactions are shown as dash lines (black). (Bottom) Structural comparison of the allosteric site with $Mg^{2+}$ and NTPs. The r6 regulatory chain of ATCase with (D) ATP•$Mg^{2+}$•ATP, (E) CTP•$Mg^{2+}$•UTP, and (F) UTP•$Mg^{2+}$•UTP bound in the A and B subsites. For clarity, Asp19 is shown but not labeled. The $Mg^{2+}$ is shown as a gray sphere and coordinated ligand interactions are shown with magenta lines. Hydrogen-bonding interactions are shown as dash lines (black). Water ligands to $Mg^{2+}$ are shown as red spheres. For clarity the first 10 residues of each regulatory chain are not shown. This figure was generated using CHIMERA.[27]

The allosteric site of the $R_{PALA}$•UTP•$Mg^{2+}$•UTP structure is shown in Figure 8F with UTP bound in both the A and B subsites. The interactions of UTP in the A subsite are different from those observed for CTP in the A subsite (compare Figures 8E and 8F). In the $R_{PALA}$•UTP•$Mg^{2+}$•UTP structure the phosphates portion of UTP in the A subsite make the same interactions with His20 and Lys94 as ATP and CTP do. However, comparing the interactions between the pyrimidine rings of CTP and UTP, UTP has only half the number of interactions that CTP has in the A subsite. There is a polar interaction between Lys60 and the 2-keto oxygen of both CTP and UTP, but the 4-keto group of UTP is unable to hydrogen bond with the backbone carbonyls of Tyr89 and Ile12. Since the pyrimidine ring of UTP is not held as strongly, it is somewhat displaced relative to CTP, which may explain the inability of UTP•$Mg^{2+}$ to inhibit the enzyme. This displacement prevents an interaction between the uridine N3 and the backbone of Ile12. The uridine of the UTP in the B subsite is held by two interactions, each to the ε-amino group of Lys60 (see Figure 8F). The majority of the binding affinity comes from interactions of the triphosphate with the $Mg^{2+}$ and the side chains of His20, Ser50, Lys56 and the backbone of Glu52. The side chain of Asp19 also has a water-mediated interaction that further adds to the triphosphate interactions (see Figure 8F).

Figure 9 compares the structural consequences of NTPs and $Mg^{2+}$ binding to the allosteric site of the regulatory chain of ATCase. In this figure the $R_{PALA}$ structure without nucleotide effectors is compared with the $R_{PALA}$•ATP•$Mg^{2+}$•ATP and the $R_{PALA}$•CTP•$Mg^{2+}$•UTP structures. ATP•$Mg^{2+}$ substantially activates the enzyme while CTP•$Mg^{2+}$•UTP causes the most inhibition. The position of the N-terminal region of the regulatory chain is altered in the $R_{PALA}$•ATP•$Mg^{2+}$•ATP structure as compared to the

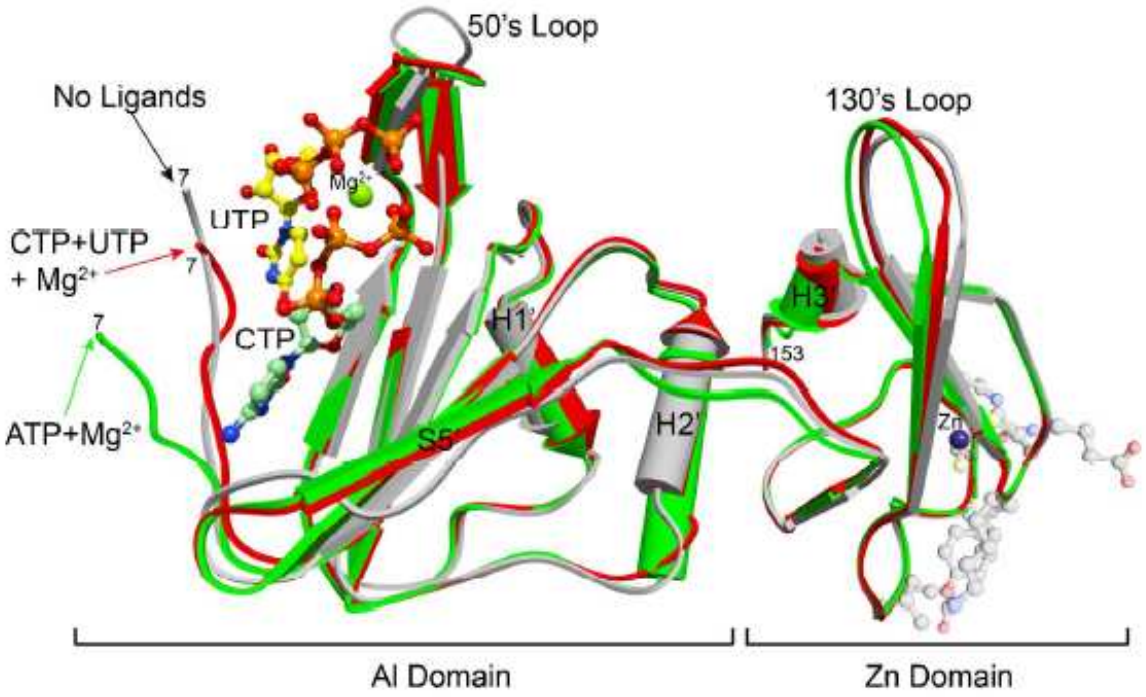


**Figure 9.** Structure changes induced by the binding of ATP + $Mg^{2+}$ (green, $R_{PALA}$•ATP•$Mg^{2+}$•ATP) or CTP + UTP + $Mg^{2+}$ (red, $R_{PALA}$•CTP•$Mg^{2+}$•UTP) to the unliganded r6 regulatory chain of ATCase in the R-state (gray, $R_{PALA}$, PDB ID 1D09). The two structures with ligands were aligned to the structure in the absence of regulatory nucleotides. For clarity the two ATPs and $Mg^{2+}$ that are bound in the $R_{PALA}$•ATP•$Mg^{2+}$•ATP are not shown, however they occupy positions very similar to CTP and UTP. The side chains of the r6 chain which interact via hydrogen bonding with the adjacent catalytic chain (c6) are shown with transparency on the right.

other two. As seen in Figure 10, the molecular basis for the alternation in position of the N-terminal region is due to the larger size of the purine ring of ATP as compared to the pyrimidine ring of UTP in the B subsite. In the $R_{PALA}$•CTP•$Mg^{2+}$•UTP structure the carbonyl oxygen at the 2 position and the nitrogen at the 3 position of the pyrimidine ring interact with the backbone of Val9. However, in the $R_{PALA}$•ATP•$Mg^{2+}$•ATP structure the purine ring of the ATP in the B subsite fits into the site by displacing the N-terminal, the escalated consequence of which might induce the interchain interaction of the N-termini.

Both structures with NTPs and $Mg^{2+}$ have a significant shift in the 50's loop region, as residues from this loop (Ser50, Glu52, Lys56) interact with the NTP in the B subsite. Strand S5', part of the five stranded sheet in the Al domain that bridges to the Zn domain, is shifted in both structures with NTPs and $Mg^{2+}$ as compared to the R•PALA structure. In the interface between the Al-Zn domains (strand S5' and helix H2') the shifts in the R•PALA•ATP•$Mg^{2+}$•ATP and the R•PALA•CTP•$Mg^{2+}$•UTP structures are in opposite directions. This alteration in the Al-Zn interface alters hydrophobic contacts that previously have been shown to be important for the allosteric regulation.[28, 29] In the case of ATP+$Mg^{2+}$ bound structure, helix H1 and helix H2 show less separation from each other compared to that of no ligand or CTP+UTP+$Mg^{2+}$ bound structures. The signal of ATP+$Mg^{2+}$ binding might exert long-range effect to perturb the orientation of two helixes, causing the hydrophobic area in between contracted. Notable is the lack of significant structural motions in the region around the structural Zn ion in the Zn domain, the region of the Zn domain that interacts with the adjacent catalytic chain, indicating that the binding of nucleotides effectors doesn't pass from regulatory chain to catalytic chain through alteration in structure of interface of zinc domain and CP domain. The C-

terminal helix (Helix H3') undergoes a dramatic reorientation resulting in alterations to the position of the C-terminus of the regulatory chain. Helix H3 includes His147r, Asn148r and Val149r. In CTP+UTP+$Mg^{2+}$ structure, the carbonyl group on the carboxamide side chain of Asn148r forms a salt link with the nitrogen atom on the imidazole ring of His147r. In ATP+$Mg^{2+}$ structure, helix H3 pivoted towards the hydrophobic pocket, which might due to the hydrophobic pocket contraction resulted from ATP+$Mg^{2+}$ binding. Alongside the carboxamide side chain of Asn148r shifted and formed salt link with His147r by its amino group instead of the carbonyl group. The interactions between the C-terminus of the r1 chain and the c4 catalytic chain in the T state have been shown to be involved in allosteric regulation. For example, Xi et al.[30] have previously shown that the removal of two residues from the C-terminus of the regulatory chain is sufficient to abolish the ability of CTP to inhibit the enzyme.

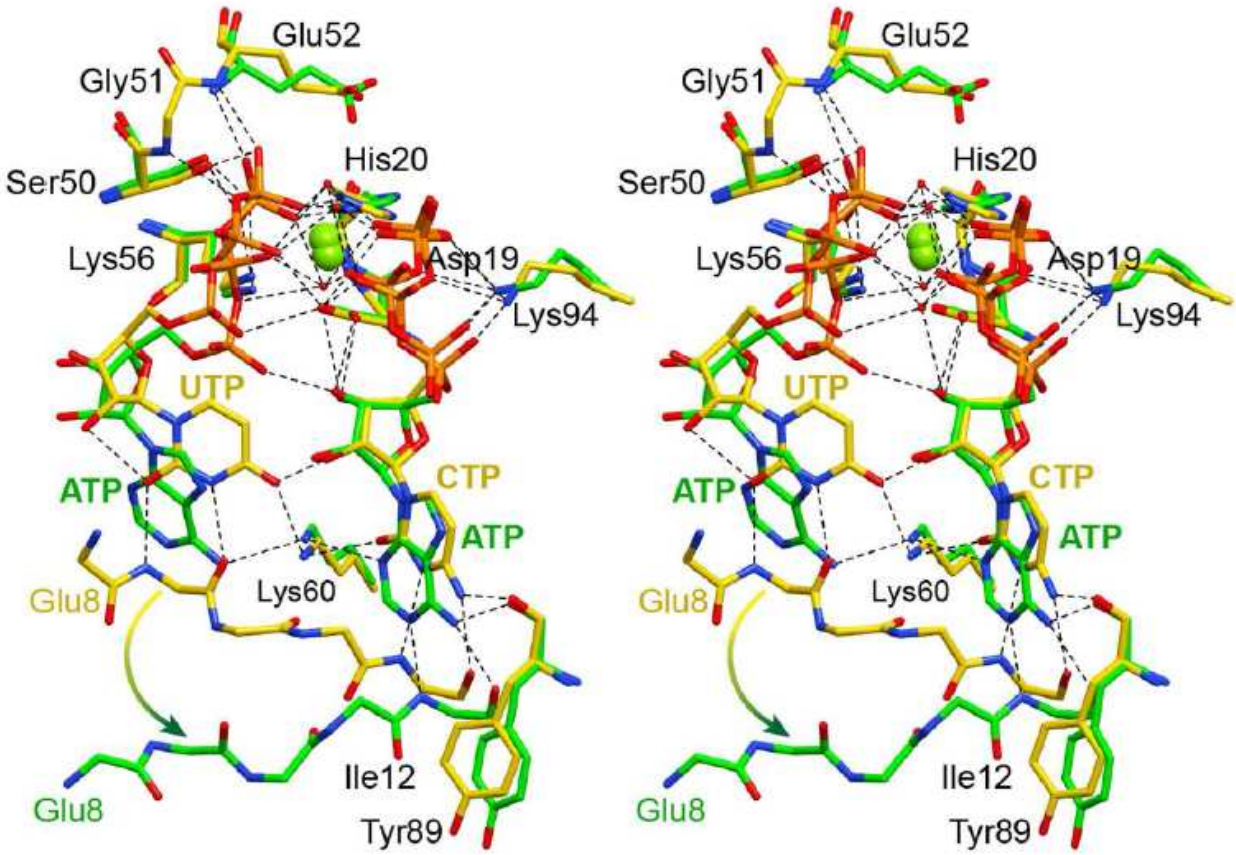


**Figure 10.** Stereoview comparison of the r6 regulatory site of ATCase from the $R_{PALA}$•ATP•$Mg^{2+}$•ATP (green carbons) and the $R_{PALA}$•CTP•$Mg^{2+}$•UTP (yellow carbons) structures. Hydrogen bonding interactions are shown with dotted lines. The arrow indicates the motion of the segment of the N-terminal shown.

**Comparison of the Solution and Crystal structures of ATCase•PALA Complex in the Presence of ATP and $Mg^{2+}$•ATP**

Structural information on the R-state of ATCase in the presence of ATP and ATP•$Mg^{2+}$ has been obtained using small-angle X-ray scattering in solution (SAXS). Fetler and Vachette[20] showed that the solution structure of ATCase•PALA ($R_{SOL}$) was altered in the presence of ATP, and in the presence of ATP•$Mg^{2+}$ to a larger extent. The SAXS data was then used to model the structures of the ATCase•PALA complex in the presence of ATP ($R_{SOL}$•ATP) and ATP•$Mg^{2+}$ ($R_{SOL}$•ATP•$Mg^{2+}$). The $R_{SOL}$•ATP and the $R_{SOL}$•ATP•$Mg^{2+}$ modeled structures were elongated along the 3-fold axis 2.8 Å and 4.4 Å more than the $R_{PALA}$ crystal structure. Furthermore, the catalytic subunits of the $R_{SOL}$•ATP and the $R_{SOL}$• ATP•$Mg^{2+}$ structures rotated 8° and 13° more around the 3-fold axis and the regulatory subunits rotated 9° and 15° more around their respective 2-fold axes, respectively, than the $R_{PALA}$ crystal structure.

The structural changes proposed by Fetler and Vachette[20] are not observed when comparing the $R_{PALA}$ crystal structure obtained in the absence of nucleotides[13] with the $R_{PALA}$•ATP and the $R_{PALA}$•ATP•$Mg^{2+}$•ATP crystal structures reported here. For both the $R_{PALA}$•ATP and $R_{PALA}$•ATP•$Mg^{2+}$•ATP structures, neither the expansion along the 3-fold axis nor the rotations of the subunits around the 3-fold and 2-fold axes differ significantly from that observed for the $R_{PALA}$ structure without allosteric effectors. The structural models determined based on the SAXS data[20] are inconsistent with the crystal structures suggesting that the structure of the enzyme in solution is different from that in crystal.

In order to investigate the discrepancy between the solution and crystal structures, we calculated SAXS profiles based on the atomic positions as determined by X-ray

crystallography. As seen in Figure 11, the calculated SAXS profile for $R_{PALA}$ without regulatory effectors is different from that calculated for the $R_{PALA}$•ATP•$Mg^{2+}$•ATP structure. The largest difference in the SAXS patterns is in the region of the first subsidiary minimum and maximum, exactly as was observed experimentally[20]However, if all the atoms constituting ATP and $Mg^{2+}$ are removed from the $R_{PALA}$•ATP•$Mg^{2+}$•ATP coordinates and the SAXS pattern is recalculated, the pattern obtained is essentially identical to the pattern calculated for the $R_{PALA}$ structure in the absence of allosteric effectors. These calculations indicate that the $R_{SOL}$•ATP and $R_{SOL}$•ATP•$Mg^{2+}$ structures of ATCase reported by Fetler and Vachette[20] are incorrect, and that the observed difference in scattering between the R-state enzyme in the absence and presence of ATP and ATP•$Mg^{2+}$ is due exclusively to the extra scattering caused by the bound ligands. These results also indicate that the solution and crystal structures of ATCase are virtually identical.

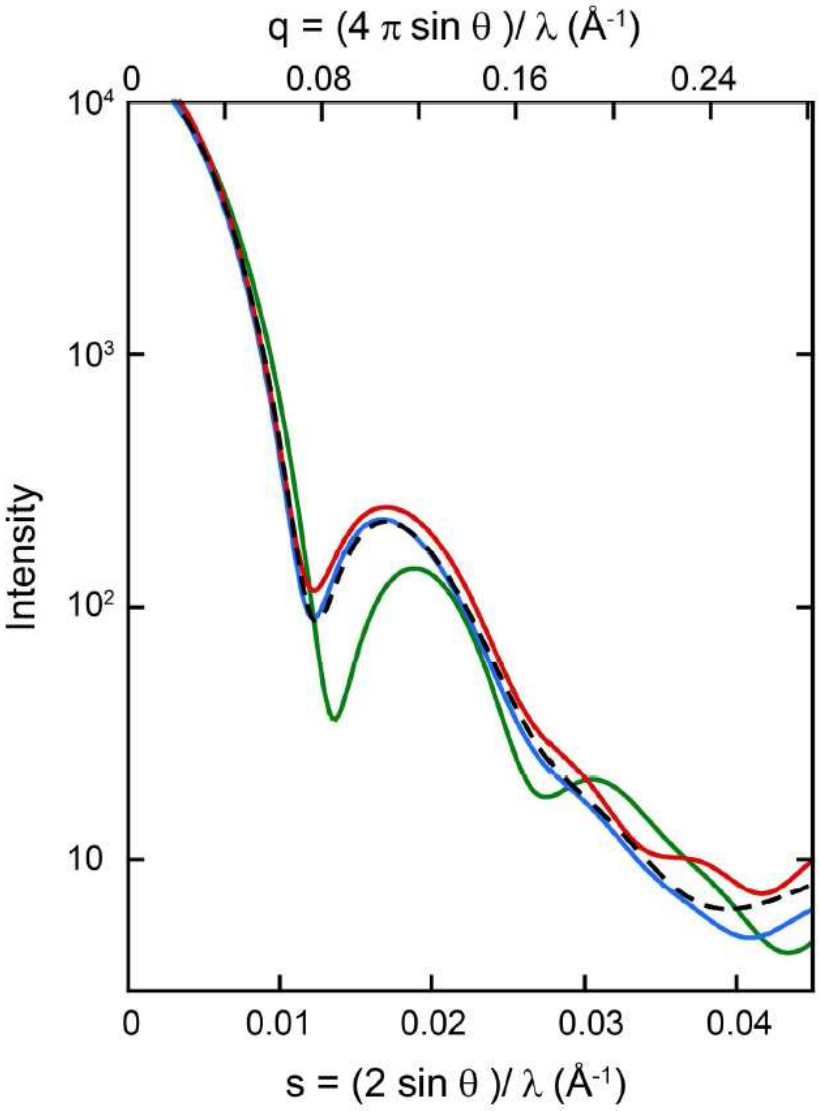


**Figure 11.** Calculated SAXS scattering curves of ATCase. SAXS profiles of the biological unit of ATCase were calculated using the FOXS Server [17] in the T-state (green, PDB ID 1ZA1 with CTP removed) and R-state with PALA (blue, PDB ID 1D09). Also shown are the calculated SAXS profiles for the $R_{PALA}$•ATP•$Mg^{2+}$•ATP structure with ligands (red) and the same structure with the ATP and $Mg^{2+}$ atoms removed (black dashed).

**Nucleotide Site Specificity**

The ATCase structures reported here confirm that the allosteric site on each regulatory chain of ATCase is actually a dinucleotide site composed of two subsites that can bind nucleotide triphosphates. Furthermore, the nucleotide that occupies each of the two independent sites must be considered in any model of allosteric regulation of ATCase. The A subsite can bind CTP, ATP, and UTP, while the B subsite can bind ATP and UTP. Although GTP has been shown to bind to the allosteric site[31], its site specificity, or lack thereof, has not been established. The simultaneous binding of two nucleotides to the A and B subsites, in any combination, is dependent upon the presence of a divalent cation. In the absence of divalent cations, ATP and CTP bind with high affinity only to the A subsite (see Figure 8A and 8B). The only NTP that is able to bind to the B subsite with reasonable affinity in the absence of divalent cations is UTP.[25]

The preferential binding of CTP to the A subsite and UTP to the B subsite is due to the interactions involving the functional group difference at the 4 position of the pyrimidine ring. The 4-keto group of uracil cannot interact with the A subsite because there are no appropriately positioned hydrogen-bond donors (see Figure 8F). However, the backbone carbonyls of Ile12 and Tyr89 serve as hydrogen-bond acceptors for the 4-amino group of the cytosine ring of CTP (see Figure 8E). The 6-amino group of adenine interacts with the same two groups on the enzyme to provide the specificity with respect to ATP (see Figure 8D).

In the presence of $Mg^{2+}$, ATP can occupy both the A and B subsites. When the two subsites are populated in this fashion the enzyme is more activated than when ATP is bound just to the A subsite (see Figure 5*)*. The combination of CTP binding at the A

subsite and UTP binding to the B subsite results in the highest level of inhibition of the enzyme. In fact, in the presence of $Mg^{2+}$, neither CTP nor UTP alone inhibits the enzyme significantly (see Figure 5). Cockrell and Kantrowitz[4] have described the selective binding of the nucleotides CTP and UTP to the A and B subsites, respectively. Part of the subsite selectivity is due to electrostatic interactions between the pyrimidine ring and Lys60, a residue that lies at the interface between the A and B subsites and has interactions with the nucleotides bound in each subsite. Therefore, an unfavorable electrostatic interaction between Lys60 and the 4-amino group of CTP precludes the binding of CTP to the B subsite. It is likely that the CTP•$Mg^{2+}$ complex has a lower binding affinity to the allosteric site than CTP, and explains why 2 mM CTP•$Mg^{2+}$ does not inhibit the enzyme. The structural basis for the ability of ATP to bind to both the A and B subsites can also be ascribed to electrostatic interactions between ATP and Lys60. The adenine N3 of ATP in the A subsite interacts with Lys60, and in the B subsite Lys60 interacts with N7 and the 6-amino group, all of which bear a partial negative charge.[32]

**The Role of the N-termini of the Regulatory Chains of ATCase in Allosteric Regulation**

In most structures of wild-type and mutant versions of ATCase, the N-termini of the regulatory chains are disordered to a significant extent to make the determination of the atomic positions of the residues impossible. Depending upon the structure, between 1 and 10 residues have been excluded. Part of the reason for the disordered N-termini is that this part of the protein makes interactions with the nucleotide in the B subsite, structures of which have not been available. The $R_{PALA}$•CTP•$Mg^{2+}$•UTP and

$R_{PALA}$•ATP•$Mg^{2+}$•ATP structures, reported here, correspond to highly inhibited and activated forms of the enzyme, respectively. As discussed above, in these two structures the N-terminal region of the regulatory chains exhibit completely different conformations.

Shown in Figure 12A are the allosteric domains of the regulatory subunit of the $R_{PALA}$•CTP•$Mg^{2+}$•UTP structure. The N-termini of the r1 and r6 chains are parallel to one another at the dimer interface. Shown in Figure 12B are the allosteric domains of the regulatory subunit of the $R_{PALA}$•ATP•$Mg^{2+}$•ATP structure. The larger purine ring of ATP in the A subsite displaces the N-terminus of the r1 chain into the allosteric site of the r6 chain and interacts with the ATP bound in the B subsite of the r6 chain and *vice versa*. The penetration of the N-terminal region into the opposing regulatory chain positions Lys6 to help neutralize the negative charges on the two triphosphates. Additional stabilization of the nucleotide in the B subsite is provided by hydrophobic interactions with Leu7 and Val9. The crossover of the N-terminal region into the opposite regulatory chain of the dimer is particularly intriguing, as this would enhance the strength of the interface between the regulatory chains within the regulatory dimer, providing a new mode by which ATP can stabilize the R state of ATCase. The position of the N-termini in the $R_{PALA}$•CTP•$Mg^{2+}$•UTP structure would provide no added stabilization to this interface thus neutralizing the effect of ATP and by inference, destabilizing the R state.

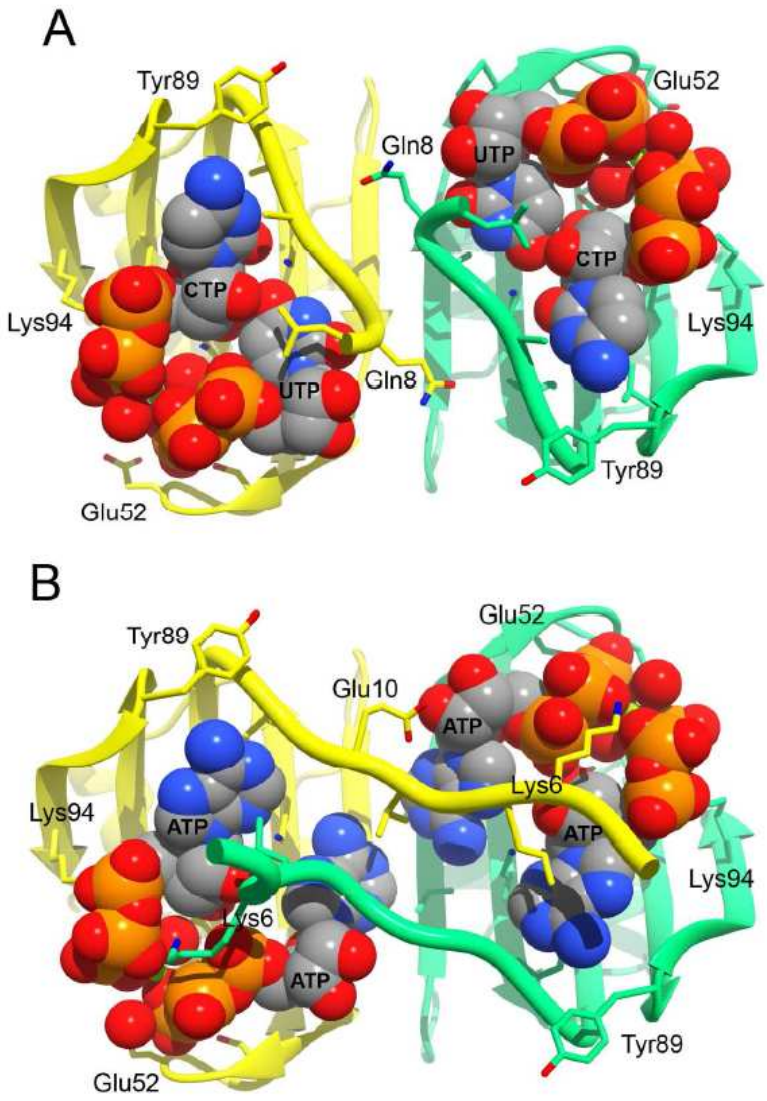


**Figure 12.** Alternate conformations of the N-terminal region. The $R_{PALA}$• CTP•$Mg^{2+}$•UTP (A) and $R_{PALA}$• ATP•$Mg^{2+}$•ATP (B) structures showing the allosteric domains of the regulatory subunit. In (A) the N-termini curl around and interact with the B subsite within their own chain, while in (B) the N-termini of one regulatory chain penetrates into B subsite of the other regulatory chain. In the $R_{PALA}$• CTP•$Mg^{2+}$•UTP and $R_{PALA}$• ATP•$Mg^{2+}$•ATP structures, 6 and 3 residues were omitted from the N-termini due to weak electron density. Figure S2 shows the relationship of the portion of the regulatory subunit shown in this figure to the holoenzyme.

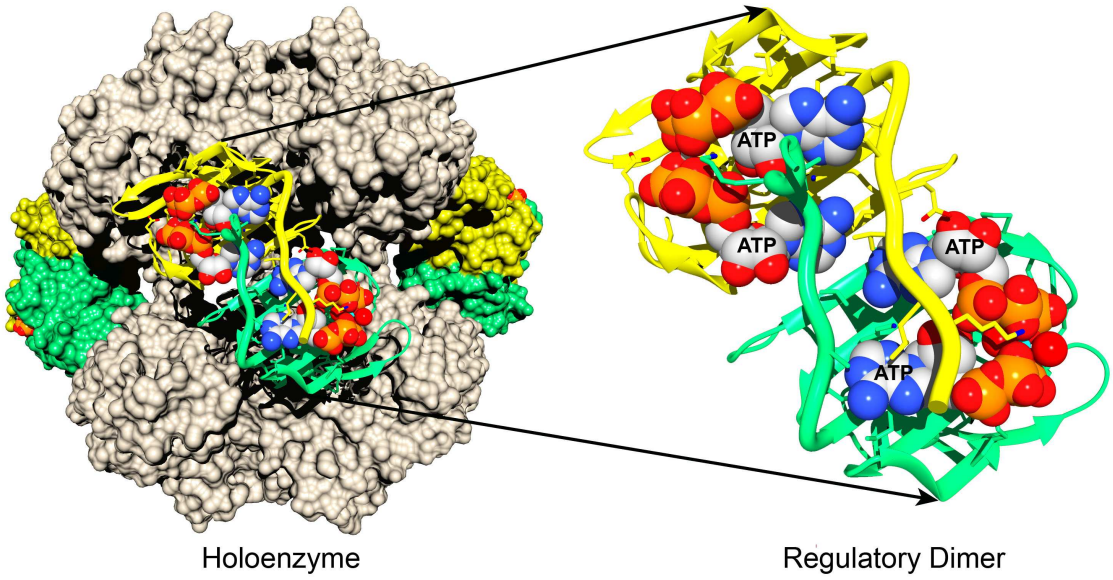


**Figure S2.** The regulatory subunit of ATCase in the context of the holoenzyme. The structure of the $R_{PALA}$•ATP•$Mg^{2+}$•ATP holoenzyme composed of two catalytic trimers and three regulatory dimers is shown on the left. The catalytic trimers (light brown) comprise the upper and lower parts of the macromolecule. Surrounding the catalytic trimers are the three regulatory dimers, with the two chains shown in green and yellow. The front most regulatory dimer is shown enlarged on the right. The two ATP molecules and the $Mg^{2+}$ in each regulatory chain are visible. The N-terminal of each regulatory chain penetrates into the allosteric site of the adjacent chain thereby strengthening the interface between the two chains of the regulatory dimer.

**Allosteric Regulation is Governed by Both Subsites in Each Regulatory Chain of ATCase**

Previous kinetic studies of single amino acid substitutions have been performed on residues identified here as involved in nucleotide binding to the A and B subsites. In the A subsite, Lys94[33] is critical for nucleotide binding. Residues that interact with the nucleotide in both subsites include Asp19, His20 and Lys60. The K60A mutation eliminates CTP inhibition and reduces the affinity of ATP. The mutant enzymes D19A[34], H20A[35], and K56A[36] lose their ability to be inhibited synergistically by UTP in the presence of CTP. The loss of synergistic inhibition could not previously be explained from a structural perspective, especially for the K56A mutation as the B subsite had not been discovered. As seen in Figure 8D, Asp19, His20 and Lys56 all provide stabilizing interactions to the ATP bound in the B subsite and have few or no interactions with CTP bound in the A subsite. Mutations at residues Asp4, Lys6, and Leu7 of the N-terminal region of the regulatory chain all influence the regulatory properties of the enzyme.[37] As seen in Figure 12, Leu7 is involved in a hydrophobic interaction with either the purine or pyrimidine ring of bound nucleotides and Lys6 helps to neutralize the charge of the two triphosphates in the $R_{PALA}$•ATP•$Mg^{2+}$•ATP structure (Figure 8D). These site-specific amino acid substitutions provide functional evidence that both the A and B subsites play a role in the allosteric regulation of ATCase.

**A New Model of Allosteric Regulation of ATCase Involving a Dinucleotide Binding Site**

Based upon the kinetics and the five X-ray structures reported here, along with the previously reported $R_{PALA}$•UTP [25], T•dCTP•$Mg^{2+}$•UTP and T•CTP•$Mg^{2+}$•UTP structures[4], a new model of allosteric regulation of ATCase can be proposed.

1) Each regulatory chain of ATCase can bind two nucleotides simultaneously, but only in the presence of a divalent cation such as $Mg^{2+}$ (see Figure 8D, 8E, and 8F).

2) Reports from the last 57 years stating that CTP is the allosteric feedback inhibitor of ATCase are inaccurate. Although CTP in the absence of divalent cations can inhibit the enzyme, in the presence of $M^{2+}$ ions at or below physiological concentrations, CTP does not significantly inhibit the enzyme. Reports from the last 24 years that ATCase is synergistically inhibited by UTP in the presence of CTP are incorrect. In the absence of metals, the combination of CTP and UTP does not inhibit the enzyme more than CTP alone (see Figure 5). In the presence of a $Mg^{2+}$, $Ca^{2+}$ or $Zn^{2+}$ at concentrations less than intracellular (2 mM), CTP does not significantly inhibit ATCase (see Figure 5 and Tables S1 and S2). In the presence of $Mg^{2+}$, $Ca^{2+}$ or $Zn^{2+}$ at concentrations below physiological, the allosteric inhibitor of ATCase is the combination CTP•$M^{2+}$•UTP with CTP binding to the A subsite and UTP binding to the B subsite. Thus, both end products of the pyrimidine pathway, CTP and UTP, act together to feedback inhibit ATCase.

3) Although ATCase can be activated by the binding of ATP in the absence of divalent cations, the enzyme can be activated to a larger extent by ATP•$M^{2+}$. Although GTP was never thought to play a significant role in allosteric regulation of ATCase, it can

function in conjunction with ATP•$Mg^{2+}$ (see Figure 5 and 6). Thus, both end products of the purine pathway, ATP and GTP can act together to allosterically activate ATCase.

4) The conformation of the N-termini of the regulatory chains is governed by the nucleotides bound in the A and B subsites. The inhibited form of the enzyme with CTP•$Mg^{2+}$•UTP bound exhibits an intrachain orientation of the N-termini, while the activated form of the enzyme with ATP•$Mg^{2+}$•ATP bound exhibits an interchain orientation of the N-termini. Thus, the activated form of the enzyme has increased stabilization of the interface between the two chains of the regulatory dimer, suggesting that these interfaces are functionally important for the stabilization of the T and R states of ATCase. This selective stabilization of the T and R states provides an explanation for how the nucleotides function in the activation and inhibition of ATCase that is consistent with the model of allostery proposed by Monod, Wyman and Changeux [38].

**REFERENCES**


1. Gerhart, J. C., and Pardee, A. B. (1962) Enzymology of control by feedback inhibition, *J. Biol. Chem. 237*, 891-896.
2. Nowlan, S. F., and Kantrowitz, E. R. (1985) Superproduction and rapid purification of *E. coli* aspartate transcarbamoylase and its catalytic subunit under extreme derepression of the pyrimidine pathway, *J. Biol. Chem. 260*, 14712-14716.
3. Baker, D. P., and Kantrowitz, E. R. (1993) The conserved residues glutamate-37, aspartate-100 and arginine-269 are important for the structural stabilization of *Escherichia coli* aspartate transcarbamoylase, *Biochemistry 32*, 10150-10158.
4. Cockrell, G. M., and Kantrowitz, E. R. (2012) Metal Ion Involvement in the Allosteric Mechanism of *Escherichia coli* Aspartate Transcarbamoylase, *Biochemistry 51*, 7128-7137.
5. Gerhart, J. C., and Holoubek, H. (1967) The purification of aspartate transcarbamylase of *Escherichia coli* and separation of its protein subunits, *J. Biol. Chem. 242*, 2886-2892.
6. Bock, R. M., Ling, N. S., Morell, S. A., and Lipton, S. H. (1956) Ultraviolet absorption spectra of adenosine-5'-triphosphate and related 5'-ribonucleotides, *Arch. Biochem. Biophys. 62*, 253-264.
7. Pastra-Landis, S. C., Foote, J., and Kantrowitz, E. R. (1981) An improved colorimetric assay for aspartate and ornithine transcarbamylases, *Anal. Biochem. 118*, 358-363.

8. Gerhart, J. C., and Pardee, A. B. (1963) The effect of the feedback Inhibitor CTP, on subunit interactions in aspartate transcarbamylase, *Cold Spring Harbor Symp. Quant. Biol. 28*, 491-496.

9. Wild, J. R., Loughrey-Chen, S. J., and Corder, T. S. (1989) In the presence of CTP, UTP becomes an allosteric inhibitor of aspartate transcarbamylase, *Proc. Natl. Acad. Sci. U. S. A. 86*, 46-50.

10. Krause, K. L., Voltz, K. W., and Lipscomb, W. N. (1987) 2.5 Å structure of aspartate carbamoyltransferase complexed with the bisubstrate analog N-(phosphonacetyl)-L-aspartate, *J. Mol. Biol. 193*, 527-553.

11. Otwinowski, Z., and Minor, W. (1997) Processing of X-ray diffraction data collected in oscillation mode, in *Methods Enzymol.* (Carter Jr., C. W., and Sweet, R. M., Eds.), pp 307-326, Academic Press, NY.

12. Pflugrath, J. W. (1999) The finer things in X-ray diffraction data collection, *Acta Cryst. D55*, 1718-1725.

13. Jin, L., Stec, B., Lipscomb, W. N., and Kantrowitz, E. R. (1999) Insights into the mechanism of catalysis and heterotropic regulation of *E. coli* aspartate transcarbamoylase based upon a structure of enzyme complexed with the bisubstrate analog N-phosphonacetyl-L-aspartate at 2.1 Å, *Proteins: Struct. Funct. Genet. 37*, 729-742.

14. Adams, P. D., Afonine, P. V., Bunkóczi, G., Chen, V. B., Davis, I. W., Echols, N., Headd, J. J., Hung, L.-W., Kapral, G. J., Grosse-Kunstleve, R. W., McCoy, A. J., Moriarty, N. W., Oeffner, R., Read, R. J., Richardson, D. C., Richardson, J. S.,

Terwilliger, T. C., and Zwart, P. H. (2010) PHENIX: a comprehensive Python-based system for macromolecular structure solution, *Acta Cryst. D66*, 213-221.

15. Emsley, P., Lohkamp, B., Scott, W. G., and Cowtan, K. (2010) Features and Development of Coot, *Acta Cryst. D66*, 486-501.

16. Laskowski, R. A., MacArthur, M. W., Moss, D. S., and Thornton, J. M. (1993) PROCHECK: A program to check the stereochemical quality of protein structures., *J. Appl. Cryst. 26*, 283-291.

17. Schneidman-Duhovny, D., Hammel, M., and Sali, A. (2010) FoXS: a web server for rapid computation and fitting of SAXS profiles, *Nucleic acids research 38 Suppl*, W540-544.

18. Christopherson, R. I., and Finch, L. R. (1977) Regulation of aspartate carbamoyltransferase of *Escherichia coli* by the interrelationship of magnesium and nucleotides, *Biochim. Biophys. Acta 481*, 80-85.

19. Honzatko, R. B., Lauritzen, A. M., and Lipscomb, W. N. (1981) Metal cation influence on activity and regulation of aspartate carbamoyltransferase, *Proc. Natl. Acad. Sci. U. S. A. 78*, 898-902.

20. Fetler, L., and Vachette, P. (2001) The allosteric activator Mg-ATP modifies the quaternary structure of the R-state of *Escherichia coli* aspartate transcarbamylase without altering the TR equilibrium, *J. Mol. Biol. 309*, 817-832.

21. Buckstein, M. H., He, J., and Rubin, H. (2008) Characterization of Nucleotide Pools as a Function of Physiological State in Escherichia coli, *Journal of bacteriology 190*, 718-726.

22. Kung, F. C., Raymond, J., and Glaser, D. A. (1976) Metal ion content of *Escherichia coli* versus cell age, *J Bacteriol. 126*, 1089-1095.

23. Kim, K. H., Pan, Z., Honzatko, R. B., Ke, H.-M., and Lipscomb, W. N. (1987) Structural asymmetry in the CTP-liganded form of aspartate carbamoyltransferase from *Escherichia coli*, *J. Mol. Biol. 196*, 853-875.

24. Stieglitz, K., Stec, B., Baker, D. P., and Kantrowitz, E. R. (2004) Monitoring the transition from the T to the R state in *E. coli* aspartate transcarbamoylase by X-ray crystallography: Crystal structures of the E50A mutant in four distinct allosteric states, *J. Mol. Biol. 341*, 853-868.

25. Peterson, A. W., Cockrell, G. M., and Kantrowitz, E. R. (2012) A second allosteric site in *E. coli* aspartate transcarbamoylase, *Biochemistry 51*, 4776-4778.

26. Gerhart, J. C. (1970) A discussion of the regulatory properties of aspartate transcarbamylase from *Escherichia coli*, *Curr. Top. Cell. Regul. 2*, 275-325.

27. Pettersen, E. F., Goddard, T. D., Huang, C. C., Couch, G. S., Greenblatt, D. M., Meng, E. C., and Ferrin, T. E. (2004) UCSF Chimera - A visualization system for exploratory research and analysis, *J. Comput. Chem. 25*, 1605-1612.

28. Van Vliet, F., Xi, X.-G., DeStaercke, C., DeWannemaeker, B., Jacobs, A., Cherfils, J., Ladjimi, M. M., Hervé, G., and Cunin, R. (1991) Heterotropic interactions in aspartate transcarbamoylase: Turning allosteric ATP activation into inhibition as a consequence of a single tyrosine to phenylalanine Mutation, *Proc. Natl. Acad. Sci. USA 88*, 9180-9183.

29. Xi, X.-G., DeStaercke, C., Van Vliet, F., Triniolles, F., Jacobs, A., Stas, P. P., Ladjimi, M. M., Simon, V., Cunin, R., and Hervé, G. (1994) The activation of *Escherichia coli* aspartate transcarbamylase by ATP: Specific involvement of helix H2' at the hydrophobic interface between the two domains of the regulatory chains, *J. Mol. Biol. 242*, 139-149.

30. Xi, X.-G., Van Vliet, F., Ladjimi, M. M., DeWannemaeker, B., DeStaercke, C., Glansdorff, N., Piérard, A., Cunin, R., and Hervé, G. (1991) The heterotropic interactions in aspartate transcarbamoylase: subunit interfaces involved in CTP inhibition and ATP activation, *J. Mol. Biol. 220*, 789-799.

31. Mendes, K. R., Martinez, J. A., and Kantrowitz, E. R. (2010) Asymmetric allosteric signaling in aspartate transcarbamoylase, *ACS Chem. Biol. 5*, 499-506.

32. Abraham, R. J., and Smith, P. E. (1988) Charge calculations in molecular mechanics 6: the calculation of partial atomic charges in nucleic acid bases and the electrostatic contribution to DNA base pairing, *Nucleic acids research 16*, 2639-2657.

33. Zhang, Y., Ladjimi, M. M., and Kantrowitz, E. R. (1988) Site-directed mutagenesis of a residue located in the regulatory site of *Escherichia coli* aspartate transcarbamylase., *J. Biol. Chem. 263*, 1320-1324.

34. Zhang, Y., and Kantrowitz, E. R. (1991) The synergistic inhibition of *Escherichia coli* aspartate carbamoyltransferase by UTP in the presence of CTP is due to the binding of UTP to the low affinity CTP sites, *J. Biol. Chem. 266*, 22154-22158.

35. Zhang, Y., and Kantrowitz, E. R. (1992) Probing the regulatory site of *Escherichia coli* aspartate transcarbamoylase by site-specific mutagenesis, *Biochemistry 31*, 792-798.

36. Corder, T. S., and Wild, J. R. (1989) Discrimination between nucleotide effector responses of aspartate transcarbamoylase due to a singe site substitution in the allosteric binding sIte, *J. Biol. Chem. 264*, 7425-7430.

37. Dembowski, N. J., and Kantrowitz, E. R. (1994) The use of alanine scanning mutagenesis to determine the role of the amino terminus of the regulatory chain in the heterotropic mechanism of *Escherichia coli* aspartate transcarbamoylase, *Protein Eng. 7*, 673-679.

38. Monod, J., Wyman, J., and Changeux, J. P. (1965) On the Nature of Allosteric Transitions: A Plausible Model, *J. Mol. Biol. 12*, 88-118.

39. Zhang, Y., and Kantrowitz, E. R. (1989) Lysine-60 in the regulatory chain of *Escherichia coli* aspartate transcarbamylase is important for the discrimination between CTP and ATP, *Biochemistry 28*, 7313-7318.